Primordial Black Holes and their Mass Spectra: The Effects of Mergers and Accretion within Stasis Cosmologies

Keith R. Dienes,[1,2,*] Lucien Heurtier,[3,†] Fei Huang,[4,‡] Tim M.P. Tait,[5,§] Brooks Thomas[6,¶]

[1] *Department of Physics, University of Arizona, Tucson, AZ 85721 USA*
[2] *Department of Physics, University of Maryland, College Park, MD 20742 USA*
[3] *Theoretical Particle Physics and Cosmology, King's College London, Strand, London WC2R 2LS, United Kingdom*
[4] *Department of Particle Physics and Astrophysics, Weizmann Institute of Science, Rehovot 7610001, Israel*
[5] *Department of Physics and Astronomy, University of California, Irvine, CA 92697 USA*
[6] *Department of Physics, Lafayette College, Easton, PA 18042 USA*

A variety of processes in the very early universe can give rise to a population of primordial black holes (PBHs) with an extended mass spectrum. For certain mass spectra of this sort, it has been shown that the evaporation of these PBHs into radiation can drive the universe toward an epoch of cosmological stasis which can persist for a significant number of e-folds of cosmological expansion. However, in general, the initial mass spectrum which characterizes a population of PBHs at the time of production can subsequently be distorted by processes such as mergers and accretion. In this paper, we examine the effects that these processes have on the spectra that lead to a PBH-induced stasis. Within such stasis models, we find that mergers have only a negligible effect on these spectra within the regime of interest for stasis. We likewise find that the effect of accretion is negligible in many cases of interest. However, we find that the effect of accretion on the PBH mass spectrum is non-negligible in situations in which this spectrum is particularly broad. In such situations, the stasis epoch is abridged or, in extreme cases, does not occur at all. Thus accretion plays a non-trivial role in constraining the emergence of stasis within scenarios which lead to extended PBH mass spectra.

CONTENTS

* Email address: dienes@arizona.edu
† Email address: lucien.heurtier@kcl.ac.uk
‡ Email address: fei.huang@weizmann.ac.il
§ Email address: ttait@uci.edu
¶ Email address: thomasbd@lafayette.edu

I. INTRODUCTION

Primordial black holes (PBHs) — *i.e.*, black holes which are not produced via stellar dynamics — can be generated by a number of processes within the early universe (for reviews, see, *e.g.*, Refs. [1, 2]). The existence of such objects can have a variety of implications for early-universe cosmology. PBHs can contribute to the present-day dark-matter abundance [3, 4] and serve as engines for the production of dark-matter particles [5–12] or of heavy, unstable particles whose baryon-number-violating decays contribute to the generation of a baryon asymmetry for the universe [5, 6, 9].

PBHs can also potentially have an impact on the expansion history of the universe (for reviews, see, *e.g.*, Ref. [13]). For example, a population of PBHs can come to dominate the energy density of the universe prior to the Big-Bang nucleosynthesis (BBN) epoch, thereby giving rise to an early matter-dominated era. Alternatively, a cosmological population of black holes with an extended mass spectrum can even give rise to a situation in which the abundances of matter and radiation remain effectively constant for a significant duration [14, 15]. In other words, such a population of PBHs furnishes a realization of *cosmological stasis* [16, 17] — a phenomenon wherein energy density is transferred from cosmological energy components with smaller equation-of-state parameters to those with larger equation-of-state parameters in such a way as to precisely compensate for the differing manner in which the energy densities associated with these individual components are affected by cosmic expansion, thereby resulting in constant abundances for these different energy components despite the expansion of the universe. In this realization of the stasis phenomenon, PBH evaporation via the emission of Hawking radiation is the mechanism which facilitates the transfer of energy density from matter to radiation. Indeed, within this realization of stasis, it can be shown that the stasis state is a global dynamical attractor [14, 15], just as it is within the many other stasis cosmologies that have been shown to exist [16–24]. Thus, even though their initial conditions may vary widely, such PBH cosmologies are inevitably drawn towards a stasis configuration in which the effects of Hawking radiation and cosmological expansion are precisely balanced against each other. Moreover, realizations of stasis involving PBHs can give rise to distinctive phenomenological signatures, including characteristic imprints on the stochastic gravitational-wave background [15].

This stasis-inducing interplay between cosmological expansion and PBH evaporation is ultimately sensitive to the manner in which the differential number density $f_{\rm BH}(M,t)$ for the population of PBHs scales with the PBH mass M across the extended PBH spectrum. In situations in which these two processes are the only ones that have a non-negligible impact on the evolution of $f_{\rm BH}(M,t)$, the PBH mass spectrum evolves with time in a particularly simple manner. Cosmological expansion reduces the physical number density of PBHs, thereby decreasing the overall *normalization* of $f_{\rm BH}(M,t)$ but leaving the *shape* of $f_{\rm BH}(M,t)$ intact. By contrast, over time, evaporation effectively converts the (matter) energy density associated with PBHs into radiation. This process is actually quite abrupt — far more so than, *e.g.*, the exponential decay of a population of unstable particles — in the sense that the vast majority of the initial mass of a given PBH is converted into radiation within a comparatively short time interval immediately prior to the time at which the PBH evaporates completely. Evaporation therefore does not have a significant impact on the shape of $f_{\rm BH}(M,t)$ at values of M significantly larger than the mass of the lightest PBH which has yet to evaporate at time t.

By contrast, in situations in which additional processes have a non-negligible impact on the time-evolution of $f_{\rm BH}(M,t)$, the initial shape of this differential number density can be distorted over time. Such distortions can potentially disrupt the dynamics which gives rise to stasis. As it turns out, the two processes which have the greatest potential to alter the shape of $f_{\rm BH}(M,t)$ in this way are the accretion of material onto the PBHs and mergers between PBHs.

In this paper, we shall therefore examine the effects that mergers and accretion have on $f_{\rm BH}(M,t)$ in PBH-induced-stasis scenarios. To do this, we shall consider the PBH-induced stasis model presented in Ref. [15] and identify those parameter-space regions associated with this model within which mergers and accretion are unimportant across the entire PBH mass spectrum. These are therefore regions of parameter space within which the stasis-inducing dynamics is essentially undisturbed. We shall also identify those regions in which these effects might lead to more significant distortions.

Our primary results can be summarized as follows. As we shall find, the effects of mergers on $f_{\rm BH}(M,t)$ are negligible across the entire region of parameter space relevant for stasis. Thus the effects of mergers are ultimately not a concern for the stasis-inducing dynamics in Ref. [15]. By contrast, whether or not the effects of accretion have a significant impact on $f_{\rm BH}(M,t)$ depends on the location in parameter space. Throughout the vast majority of the parameter space relevant for stasis — and indeed the majority of that parameter space wherein the prospects for detecting the distinctive phenomenological signatures identified in Ref. [15] are particularly auspicious — the effects of accretion are also negligible. Thus, throughout much of the stasis-producing parameter space associated with the model of Ref. [15], the dynamics leading to stasis is largely unaffected by either mergers or accretion. However, within certain regimes — in particular, those in which the PBH mass spectrum is almost maximally broad or in which the PBHs collectively dominate the energy density of the universe for a significant duration prior to stasis — accretion can have a more significant impact on $f_{\rm BH}(M,t)$. In such situations, the duration of the stasis epoch can be reduced. Indeed, in extreme cases of this sort, we find that stasis might not occur at all.

This paper is organized as follows. In Sect. II, we briefly review the model of PBH-induced stasis presented in Ref. [15] and the cosmological expansion history associated with this model. In Sect. III, we then examine the process through which pairs of PBHs form binaries within the context of this cosmology. In Sect. IV, we consider the statistical properties of such PBH binaries and derive an expression for the overall rate at which the PBHs within these binaries coalesce into heavier black holes. In Sect. V, we then investigate the impact that PBH mergers have on $f_{\rm BH}(M,t)$ within the parameter-space regions relevant for stasis. In Sect. VI, we consider the effects of accretion on the evolution of $f_{\rm BH}(M,t)$ and assess how these effects impact the duration of stasis within different stasis-producing parameter-space regions. Finally, in Sect. VII, we conclude with a summary of our main results and a discussion of possible directions for future work. Appendix A provides a derivation of the probability densities associated with different configurations of PBHs which give rise to binaries with different total masses and geometries.

II. PRELIMINARIES

A population of non-relativistic Schwarzschild PBHs in the early universe may be characterized at a given cosmological time t by their differential number density $f_{\rm BH}(M,t)$ per unit PBH mass M. In general, the Boltzmann equation which describes the manner in which

$f_{\rm BH}(M,t)$ evolves may be written as

$$\begin{aligned}\frac{df_{\rm BH}(M,t)}{dt} &= -3Hf_{\rm BH}(M,t) \\ &+ \frac{\partial f_{\rm BH}(M,t)}{\partial M}\left[\left(\frac{dM}{dt}\right)_e + \left(\frac{dM}{dt}\right)_{\rm acc}\right] \\ &+ \left[\Gamma_+(M,t) - \Gamma_-(M,t)\right] f_{\rm BH}(M,t) \ , \end{aligned} \tag{2.1}$$

where $H \equiv \dot{a}/a$ is the Hubble parameter, where $(dM/dt)_e$ and $(dM/dt)_{\rm acc}$ respectively denote the rates at which M itself changes due to the emission of Hawking radiation and due to the accretion of material around it, and where the products $\Gamma_+(M,t)f_{\rm BH}(M,t)$ and $\Gamma_-(M,t)f_{\rm BH}(M,t)$ respectively denote the rates at which $f_{\rm BH}(M,t)$ changes due to the production of PBHs of mass M via the mergers of lighter PBHs and due to the disappearance of PBHs of mass M via their mergers with other PBHs. Parametrizing the merger rates in terms of $\Gamma_\pm(M,t)$, which have units of inverse time, facilitates comparison between these quantities and H, thereby providing a transparent method of assessing whether mergers have a significant effect on the differential number density of PBHs at any given point in the cosmological history. In particular, at any time at which either $\Gamma_+(M,t)$ or $\Gamma_-(M,t)$ is comparable to or larger than H for any particular value of M, the effect of mergers on $f(M,t)$ at that value of M cannot be neglected. By contrast, at any time at which $\Gamma_+(M,t)$ and $\Gamma_-(M,t)$ are both significantly smaller than H for a particular value of M, the effect of mergers on $f_{\rm BH}(M,t)$ at that value of M is insignificant.

The quantities $\Gamma_+(M,t)$ and $\Gamma_-(M,t)$, to which we shall henceforth refer as the PBH production and destruction rates from mergers, respectively, both depend non-trivially on the full functional form of $f_{\rm BH}(M,t)$. Indeed, mergers between PBHs of mass M and PBHs of any mass contribute to $\Gamma_-(M,t)$, while mergers between any two PBHs whose masses sum to M contribute to $\Gamma_+(M,t)$. The functional form of $f_{\rm BH}(M,t)$ at any given time in turn depends both on its initial form $f_{\rm BH}(M,t_i)$ at the time t_i at which the cosmological population of PBHs in question is effectively established and on the expansion history of the universe at times between t_i and t. Thus, before we begin to evaluate $\Gamma_\pm(M,t)$ within the context of PBH-induced stasis scenario put forth in Ref. [15], we briefly review the non-standard expansion history associated with this scenario and the properties of the corresponding cosmological population of PBHs.

A. Mass Spectrum

One mechanism through which a cosmological population of PBHs with an extended mass spectrum can be generated within the early universe is via the collapse of primordial density perturbations after inflation. The relationship between the initial mass M_i of a PBH and the time $t_p(M_i)$ at which it is produced in this way is given by (for reviews, see, *e.g.*, Ref. [25])

$$M_i = \frac{4\pi}{3}\gamma\frac{\rho_{\rm crit}(t_p)}{H^3(t_p)} \ , \tag{2.2}$$

where $H(t)$ is the Hubble parameter at time t and where γ is an $\mathcal{O}(1)$ proportionality factor which depends on the details of the collapse dynamics. In what follows, we take $\gamma = 1$, though we emphasize that our results are not particularly sensitive to the value of γ. Since Eq. (2.2) implies that $t_p(M_i)$ is a monotonically increasing function of M_i, it follows that the production of PBHs ends at the time $t_i \equiv t_p(M_{\rm max})$ at which the PBHs with the maximum initial mass $M_{\rm max}$ are produced.

Once a PBH is produced, it begins losing mass via the emission of Hawking radiation. The rate of change of M due to evaporation is [26, 27]

$$\left(\frac{dM}{dt}\right)_e \equiv -\varepsilon(M)\frac{M_P^4}{M^2} \ , \tag{2.3}$$

where $M_P \equiv G^{-1/2}$ is the Planck mass, defined in terms of Newton's constant G, and where the evaporation function $\varepsilon(M)$ characterizes how this rate varies with M. As discussed in Ref. [15], $\varepsilon(M) \approx \varepsilon$ is effectively independent of M within our regime of interest for stasis. For such a mass-independent evaporation function, Eq. (2.3) implies that the time $\tau_e(M_i)$ at which a PBH of initial mass M_i evaporates completely is

$$\tau_e(M_i) = \frac{M_i^3}{3\varepsilon M_P^4} \ . \tag{2.4}$$

Moreover, Eq. (2.3) also implies that the majority of this initial mass is lost at times comparable to $\tau_e(M_i)$. It is therefore reasonable for us to adopt an "instantaneous-evaporation" approximation wherein we take the mass $M(t)$ of a PBH at to be approximately equal to its initial mass M_i at any time $t_i < t < \tau_e(M_i)$.

We shall focus in what follows on the case in which the entire spectrum of PBHs is generated during a single cosmological epoch wherein $w = w_c$, where w_c is a constant. The initial number density $f_{\rm BH}(M_i,t_i)$ of PBHs per unit M_i which results from gravitational collapse in this case takes the form [28–32]

$$f_{\rm BH}(M_i,t_i) = \begin{cases} CM_i^{\alpha-1} & \text{for } M_{\rm min} \le M_i \le M_{\rm max} \\ 0 & \text{otherwise} \ , \end{cases} \tag{2.5}$$

where α is a power-law exponent, where C is a normalization coefficient, and where $M_{\rm min}$ denotes the minimum mass of PBHs within this population. The value of the scaling exponent α which appears in Eq. (2.5) is related to w_c by [28]

$$w_c \equiv -\frac{\alpha+1}{\alpha+3} \ . \tag{2.6}$$

The range for α which is physically motivated and also gives rise to stasis is $-2 \leq \alpha < -1$, which corresponds to the range $0 < w_c \leq 1$ [15]. For α within this range, the normalization coefficient C in Eq. (2.5) is

$$C = \frac{(\alpha+1)\rho_{\text{BH},i}}{M_{\text{max}}^{\alpha+1} - M_{\text{min}}^{\alpha+1}} , \tag{2.7}$$

where $\rho_{\text{BH},i}$ is the total initial abundance of PBHs at $t = t_i$. The values of M_{min} and M_{max} are likewise constrained by phenomenological considerations. Constraints on PBH decay from BBN [33–35] place an upper bound on M_{max} in situations in which $\rho_{\text{BH},i}$ is sufficiently large that the PBHs come to dominate the energy density of the universe at any time, while the upper bound from CMB data on the Hubble parameter during inflation [36] in turn imposes a lower bound on M_{min}. Given these constraints, we focus on combinations of M_{min} and M_{max} which satisfy

$$0.1 \text{ g} \leq M_{\text{min}} < M_{\text{max}} \leq 10^9 \text{ g} . \tag{2.8}$$

Moreover, in what follows, we shall primarily be interested in cases in which we also have $M_{\text{min}} \ll M_{\text{max}}$.

B. Expansion History

In PBH-induced stasis scenarios of the sort discussed in Ref. [15], the portion of the expansion history between the end of inflation and the time t_{MRE} of matter-radiation equality can, to a very good approximation, be divided into four distinct epochs, during each of which the effective equation-of-state parameter w is approximately constant. The first of these is the epoch during which the PBHs are produced via gravitational collapse, wherein $w = w_c$. Since $0 < w_c \leq 1$ for values of α relevant for stasis, as discussed below Eq. (2.6), ρ_{BH} grows during this epoch until the PBHs eventually come to dominate the energy density of the universe. At this point, a second epoch begins — one in which $w = 0$. The time t_f at which this the transition to this early matter-dominated epoch occurs for any given value of w_c is determined by the initial energy density $\rho_{\text{BH},i}$ at $t = t_i$.

The third epoch is the stasis epoch itself, which effectively begins at the time t_{PBH} at which the lightest PBHs in the spectrum evaporate completely. It follows from Eq. (2.4) that

$$t_{\text{PBH}} = \frac{M_{\text{min}}^3}{3\epsilon M_P^4} . \tag{2.9}$$

During this stasis epoch, the effective equation-of-state parameter for the universe is given by $w = \overline{w}$, where [15]

$$\overline{w} = -\frac{\alpha+1}{\alpha+7} . \tag{2.10}$$

The stasis epoch lasts until the time t_s at which the heaviest PBHs in the spectrum evaporate completely. Thus, it follows from Eq. (2.4) that

$$t_s = \frac{M_{\text{max}}^3}{3\epsilon M_P^4} . \tag{2.11}$$

The fourth and final epoch prior to matter-radiation equality is the usual radiation-dominated epoch, which effectively begins at t_s and lasts until t_{MRE}.

The timescales t_{PBH} and t_s associated with the beginning and end of the stasis epoch — as well as the equation-of-state parameters w_c and $\overline{w}$ during the PBH-formation and stasis epochs, respectively — are entirely determined by the parameters M_{min}, M_{max}, and α which characterize the shape of the PBH mass spectrum. By contrast, the timescale t_f associated with the beginning of the PBH-dominated epoch immediately prior to stasis also depends on $\rho_{\text{BH},i}$, which characterizes the overall normalization of this spectrum — or, equivalently, on the number of e-folds $\mathcal{N}_{\text{PBH}}$ of cosmological expansion which take place during that PBH-dominated epoch. The expansion history of our PBH-induced-stasis model is therefore completely characterized by the four free parameters M_{min}, M_{max}, α, and $\mathcal{N}_{\text{PBH}}$.

A mass spectrum of the simple form given in Eq. (2.5) arises only in situations in which all PBHs form during a single cosmological epoch with a constant equation-of-state parameter. Thus, our region of interest within the four-dimensional parameter space of this model is that wherein not only are the phenomenological constraints and consistency conditions on M_{min}, M_{max}, and α sat-

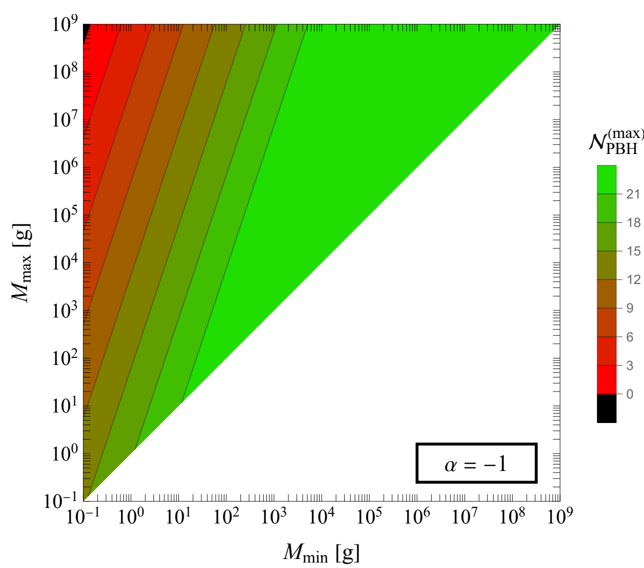

Fig. 1. Contours of the maximum value $\mathcal{N}_{\text{PBH}}^{(\text{max})}$ of $\mathcal{N}_{\text{PBH}}$ consistent with our stasis cosmology, shown in the $(M_{\text{min}}, M_{\text{max}})$-plane for $\alpha = -1$. The black region of the plot is inconsistent with our cosmology for all $\mathcal{N}_{\text{PBH}} \geq 0$ and therefore excluded. The corresponding upper bound on $\mathcal{N}_{\text{PBH}}$ is weaker for all $\alpha < -1$ throughout the entirety of the upper half-plane, though the value $\mathcal{N}_{\text{PBH}}^{(\text{max})}$ is largely insensitive to the choice of α.

isfied, but also wherein $\rho_{\mathrm{BH},i}$ is sufficiently small that the lighter PBHs within this spectrum do not collectively come to dominate the energy density of the universe before the heaviest PBHs have had a chance to form. This upper bound on $\rho_{\mathrm{BH},i}$ can equivalently be expressed as an upper bound on $\mathcal{N}_{\mathrm{PBH}}$ for any combination of M_{min}, M_{max}, and α.

In Fig. 1, we show contours within the $(M_{\mathrm{min}}, M_{\mathrm{max}})$-plane of the maximum value $\mathcal{N}_{\mathrm{PBH}}^{(\mathrm{max})}$ of $\mathcal{N}_{\mathrm{PBH}}$ consistent with this upper bound. The results shown in the figure correspond to the parameter choice $\alpha = -1$. However, the value of $\mathcal{N}_{\mathrm{PBH}}^{(\mathrm{max})}$ is not terribly sensitive to α for values of this parameter that lie within the range $-2 \leq \alpha < -1$ relevant for stasis. Moreover, we note that this insensitivity is not merely a reflection of our taking γ to be independent of w_c. Indeed, $\mathcal{N}_{\mathrm{PBH}}^{(\mathrm{max})}$ is insensitive to α regardless of the manner in which γ depends non-trivially on w_c, provided of course that this presumably $\mathcal{O}(1)$ parameter in fact remains $\mathcal{O}(1)$ across this relevant range of α.

III. BINARY CAPTURE

In general, PBH mergers proceed in two stages. First, a pair of PBHs decouples from the Hubble flow and forms a binary. Second, the binary loses energy as a result of gravitational-wave emission and the two PBHs coalesce and merge into a single, more massive black hole. Thus, in order to determine the merger rate, we must consider how the characteristic timescales associated with both stages of this process depend on the properties of the merging PBHs and on their environment. In doing so, we make extensive use of the formalism established in Ref. [37] for evaluating the merger rate of a population of PBHs with an extended mass spectrum within the standard cosmology — a formalism which we extend here to that of cosmologies with non-standard expansion histories. Throughout the remainder of this section, we shall focus exclusively on binary formation. We shall defer our discussion of the coalescence of PBHs within binaries after these binaries have formed until Sect. IV.

In the Newtonian approximation, the physical proper distance r between a pair of PBHs with masses M_1 and M_2 in a flat, Friedmann-Robertson-Walker (FRW) universe evolves according to the equation

$$\ddot{r} \;=\; -G\frac{M_B}{r^2} + \frac{\ddot{a}}{a}r \;, \tag{3.1}$$

where $M_B \equiv M_1 + M_2$ is the total mass of the system, where a is the scale factor, and where a dot denotes a derivative with respect to the coordinate time t in the cosmological background frame. From the Friedmann acceleration equation, we have

$$\frac{\ddot{a}}{a} \;=\; -\frac{4\pi G}{3}(1+3w)\rho_{\mathrm{crit}} \tag{3.2}$$

where ρ_{crit} is the critical energy density of the universe and where w is the effective equation-of-state parameter for the universe as a whole. Thus, Eq. (3.1) can be written as

$$\ddot{r} \;=\; -G\frac{M_B}{r^2} - \frac{4\pi G}{3}(1+3w)\rho_{\mathrm{crit}} r \;. \tag{3.3}$$

The time t_B at which a pair of PBHs effectively decouples from the Hubble flow can be approximated as the time at which the gravitational term in Eq. (3.3) becomes larger in magnitude than the cosmological-expansion term. In other words, t_B is given implicitly by the solution to the equation

$$M_B \;=\; \frac{4\pi}{3}(1+3w)\rho_{\mathrm{crit}}(t_B) r^3(t_B) \;. \tag{3.4}$$

At times $t \lesssim t_B$, one may approximate $r(t)$ as evolving under the influence of cosmic expansion alone. This implies that $r(t)$ evolves with the scale factor at such times according to the relation

$$r(t) \;\approx\; \frac{a(t)}{a_*} r(t_*) \;. \tag{3.5}$$

In other words, the *comoving* distance $x \equiv r(t)/a(t)$ between a pair of PBHs remains effectively constant until $t \sim t_B$.

The manner in which the critical density changes with $a(t)$ at any given time depends on the abundances and equation-of-state parameters of the individual cosmological energy components present at that time. In what follows, we shall approximate the value of w during each of these epochs as effectively constant and approximate the brief transition periods between them as instantaneous. During any individual epoch within which w remains constant, the critical density evolves with a according to the relation

$$\rho_{\mathrm{crit}}(t) \;=\; \rho_{\mathrm{crit}}(t_*) \left[\frac{a(t)}{a_*}\right]^{-3(1+w)} \;, \tag{3.6}$$

where t_* is some fiducial time during that epoch and where $a_* \equiv a(t_*)$. Combining this expression with the expression for $r(t)$ in Eq. (3.5), we find that the critical density is well approximated by

$$\rho_{\rm crit}(t)r^3(t) \;\approx\; \frac{1}{2}\rho_{\rm MRE}r^3(t_{\rm MRE})\times\begin{cases}1 & t_{\rm MRE}<t\\ \left(\frac{a}{a_{\rm MRE}}\right)^{-1} & t_s<t<t_{\rm MRE}\\ \left(\frac{a_s}{a_{\rm MRE}}\right)^{-1}\left(\frac{a}{a_s}\right)^{-3\overline{w}} & t_{\rm PBH}<t<t_s\\ \left(\frac{a_s}{a_{\rm MRE}}\right)^{-1}\left(\frac{a_{\rm PBH}}{a_s}\right)^{-3\overline{w}} & t_f<t<t_{\rm PBH}\\ \left(\frac{a_s}{a_{\rm MRE}}\right)^{-1}\left(\frac{a_{\rm PBH}}{a_s}\right)^{-3\overline{w}}\left(\frac{a}{a_f}\right)^{-3w_c} & t_{\rm end}<t<t_f\ ,\end{cases} \tag{3.7}$$

where $\rho_{\rm MRE}\equiv\rho_{\rm crit}(t_{\rm MRE})$, where $t_{\rm end}$ is the time at which inflation ends and the PBH-formation epoch begins, and where the overall factor of $1/2$ accounts for the fact that radiation represents half of the critical density at matter-radiation equality. We note that the quantity $\rho_{\rm crit}(t)r^3(t)$ has no dependence on a and remains constant throughout the PBH-domination epoch because $\rho_{\rm crit}\propto a^{-3}$ during an epoch of matter domination. This implies that a pair of PBHs which have negligible velocities in the cosmological background frame cannot undergo binary capture during the PBH-dominated epoch. Indeed, this is the case in the later matter-dominated era which follows $t_{\rm MRE}$ as well [37].

Substituting the result in Eq. (3.7) into Eq. (3.4), we find that the value of the scale factor $a_B\equiv a(t_B)$ at the time that a pair of PBHs forms a binary is

$$a_B \;=\; \begin{cases} a_{\rm MRE}\left(\frac{x}{\widetilde{x}}\right)^3 & 1>\frac{x}{\widetilde{x}}>Q_s\\ \frac{a_{\rm PBH}}{Q_{\rm PBH}^{1/\overline{w}}}\left(\frac{x}{\widetilde{x}}\right)^{1/\overline{w}} & Q_s>\frac{x}{\widetilde{x}}>Q_{\rm PBH}\\ a_{\rm PBH} & Q_{\rm PBH}>\frac{x}{\widetilde{x}}>Q_f\\ \frac{a_f}{Q_f^{1/w_c}}\left(\frac{x}{\widetilde{x}}\right)^{1/w_c} & Q_f>\frac{x}{\widetilde{x}}\end{cases} \tag{3.8}$$

where

$$\widetilde{x}\;\equiv\;\left(\frac{3M_B}{4\pi\rho_{\rm MRE}a_{\rm MRE}^3}\right)^{1/3} \tag{3.9}$$

is a fiducial distance that depends on the overall mass M_B of the binary and where we have defined

$$\begin{aligned} Q_{\rm PBH} &\equiv \left[\frac{2a_s^{1-3\overline{w}}a_{\rm PBH}^{3\overline{w}}}{(1+3\overline{w})a_{\rm MRE}}\right]^{1/3}\\ Q_f &\equiv \left[\frac{2a_s^{1-3\overline{w}}a_{\rm PBH}^{3\overline{w}}}{(1+3w_c)a_{\rm MRE}}\right]^{1/3} = \left(\frac{1+3\overline{w}}{1+3w_c}\right)^{1/3}Q_{\rm PBH}\\ Q_s &\equiv \left(\frac{a_s}{a_{\rm MRE}}\right)^{1/3}. \end{aligned} \tag{3.10}$$

These dimensionless quantities represent the normalized initial comoving separations $x/\widetilde{x}$ between two PBHs which decouple from the Hubble flow and form a binary at $t_{\rm PBH}$, t_f and t_s, respectively. We note that $Q_{\rm PBH}$, Q_f, and Q_s depend on the properties of the initial PBH mass spectrum as a whole, but not on the masses of the PBHs that constitute a particular binary.

Since w is constant during each epoch of our PBH-induced stasis cosmology, the relationship between a and t during any particular epoch is given by $a=a_*(t/t_*)^{2/(3+3w)}$, where once again t_* is some fiducial time during that epoch. Thus, it follows from Eq. (3.8) that t_B itself is given by

$$t_B \;=\; \begin{cases} t_{\rm MRE}\left(\frac{x}{\widetilde{x}}\right)^6 & Q_s<\frac{x}{\widetilde{x}}<1\\ t_{\rm PBH}\left(Q_{\rm PBH}^{-1}\frac{x}{\widetilde{x}}\right)^{(3+3\overline{w})/(2\overline{w})} & Q_{\rm PBH}<\frac{x}{\widetilde{x}}<Q_s\\ t_{\rm PBH} & Q_f<\frac{x}{\widetilde{x}}<Q_{\rm PBH}\\ t_f\left(Q_f^{-1}\frac{x}{\widetilde{x}}\right)^{(3+3w_c)/(2w_c)} & \frac{x}{\widetilde{x}}<Q_f\ .\end{cases} \tag{3.11}$$

Our expression for a_B in Eq. (3.8) for x values within the range $Q_f<x/\widetilde{x}<Q_{\rm PBH}$ deserves further comment. On the one hand, the fact that we are approximating the transitions between epochs as instantaneous and the effective equation-of-state parameter w as constant during each epoch leads to a situation in which $Q_f\neq Q_{\rm PBH}$. On the other hand, the approximations that we have employed in modeling the process of binary formation imply that a pair of PBHs cannot decouple from the Hubble flow during a matter-dominated epoch. It therefore follows that there should exist a well-defined threshold value of $x/\widetilde{x}$ for any given combination of model parameters below which a PBH pair decouples during the PBH-formation epoch and above which it decouples during the stasis epoch. Given these considerations, we take $a_B=a_{\rm PBH}$ for all PBH pairs with $Q_f<x/\widetilde{x}<Q_{\rm PBH}$, such that they decouple immediately at the moment at which the PBH-dominated epoch concludes. We emphasize that this range of $x/\widetilde{x}$ is always quite narrow within our parameter-space regime of interest. Indeed, for α within the range $-2\leq\alpha\leq-1$ relevant for stasis, we have $(2/5)^{1/3}\approx 0.737<Q_f/Q_{\rm PBH}<1$. As such, our choice of convention for handling PBH pairs with $x/\widetilde{x}$ within this narrow range does not have a significant impact on our results.

The expression in Eq. (3.8) holds at times well after the last PBHs — *i.e.*, those with the largest initial masses — are produced. At very early times, additional subtleties arise related to the manner in which the PBHs in our scenario are produced. First of all, a pair of PBHs clearly cannot form a binary before the time $t_p(M_i)$ at which the heavier of the two PBHs, whose mass is here denoted M_i, is produced. It follows from Eq. (2.2) that the scale factor $a_p(M_i) \equiv a(t_p(M_i))$ at this time is

$$a_p(M_i) \ = \ a_f \left[\frac{16\pi M_i^2 \rho_{\rm MRE}}{3\gamma^2 M_P^6} \frac{a_{\rm MRE}^4 a_s^{3\overline{w}-1}}{a_f^3 a_{\rm PBH}^{3\overline{w}}}\right]^{1/(3+3w_c)} . \tag{3.12}$$

It follows from Eq. (3.8) that the requirement that $a_B > a_p(M_i)$ can be expressed as a constraint on the initial comoving distance x between the PBHs, which takes the form

$$\frac{x}{\widetilde{x}} \ > \ Q_p \ , \tag{3.13}$$

where we have defined

$$Q_p \ \equiv \ \left[\frac{2a_s^{1-3\overline{w}} a_{\rm PBH}^{3\overline{w}} a_p^{3w_c}(M_i)}{(1+3w_c) a_{\rm MRE} a_f^{3w_c}}\right]^{1/3} \ = \ Q_f \left(\frac{a_p}{a_f}\right)^{w_c} . \tag{3.14}$$

In cases in which this constraint is not satisfied, the PBH pair would already nominally have decoupled from the Hubble flow prior to the time at which the heavier member is produced.

Moreover, since PBHs form in our scenario due to the collapse of density perturbations whose comoving wavelength $\lambda_k = 2\pi/k \sim (aH)^{-1}$ is comparable to the comoving Hubble radius, it is conceivable — and in fact quite likely — that the lighter member of any PBH pair which fails to satisfy the constraint in Eq. (3.13) will already lie within the volume of space which collapses to form the heavier member of that pair at the moment it is initially produced. When this is the case, the mass of the lighter PBH is incorporated into the mass of the heavier one as it forms. Indeed, the form of $f_{\rm BH}(M_i, t_i)$ in Eq. (2.5) accounts for this effect [28]. Since the volume of space which collapses to form a PBH of M_i is a sphere whose radius is equal to the Schwarzschild radius of that PBH, it follows that the lighter member of a would-be PBH pair can only be regarded as a distinct object after the heavier member is produced when the condition $x > x_p(M_i, M_i') \equiv 2\max\{M_i, M_i'\}G/a_p$ is satisfied, where M_i and M_i' denote the masses of two PBHs. Isolating the dependence of $x_p(M_i, M_i')$ on these masses and using the relation in Eq. (2.6) to simplify the exponent, we find that

$$\begin{aligned} x_p(M_i, M_i') \ &= \ \hat{x}\left(\frac{\max\{M_i, M_i'\}}{M_P}\right)^{(1+3w_c)/(3+3w_c)} \\ &= \ \hat{x}\left(\frac{\max\{M_i, M_i'\}}{M_P}\right)^{-\alpha/3} , \end{aligned} \tag{3.15}$$

where we have defined

$$\hat{x} \ = \ \frac{2}{M_P}\left[\frac{3\gamma^2 M_P^4}{16\pi\rho_{\rm MRE}} \frac{a_f^{-3w_c} a_{\rm PBH}^{3\overline{w}}}{a_{\rm MRE}^4 a_s^{3\overline{w}-1}}\right]^{1/(3+3w_c)} . \tag{3.16}$$

Equivalently, we note the condition $x > x_p(M_i, M_i')$ can be expressed as

$$\frac{x}{\widetilde{x}} \ > \ \chi_B(M_i, M_i') Q_p \ , \tag{3.17}$$

where

$$\chi_B(M_i, M_i') \ \equiv \ \left[\frac{(1+3w_c)\gamma^2 \max\{M_i, M_i'\}}{M_B}\right]^{1/3} \tag{3.18}$$

is a dimensionless $\mathcal{O}(1)$ quantity that depends both on the total mass of the PBH pair and on the manner in which that mass is partitioned between the two PBHs. We note that in deriving Eq. (3.18), we have used the fact that a_p can be written in terms of Q_p as

$$a_p \ = \ \frac{1}{\widetilde{x} M_P^2 Q_p}\left[\frac{8M_i^2 M_B}{\gamma^2(1+3w_c)}\right]^{1/3} . \tag{3.19}$$

Given the allowed range for w_c, we note that the allowed range for $\chi_B(M_i, M_i')$ is

$$\left(\frac{\gamma^2}{2}\right)^{1/3} \ < \ \chi_B(M_i, M_i') \ < \ (4\gamma^2)^{1/3} . \tag{3.20}$$

Thus, for $\gamma = 1$, we have $2^{-1/3} < \chi_B < 2^{2/3}$. In cases in which $\chi_B(M_i, M_i') > 1$ for any particular combination of M_i, M_i' and M_B, the lighter PBH in any PBH pair that would have decoupled from the Hubble flow prior to the formation of the heavier PBH (*i.e.*, that has $a_B < a_p$ and thus $x/\widetilde{x} < Q_p$) always lies within the Schwarzschild radius of the heavier PBH and is therefore always incorporated into that heavier PBH at the moment it forms. By contrast, in cases in which $\chi_B(M_i, M_i') < 1$, there are values of x for which the lighter PBH lies outside the Schwarzschild radius of the heavier PBH at this moment. In such cases, the decoupling condition is satisfied immediately at the moment that $x = x_p(M_i, M_i')$ and the heavier PBH forms.

In order to express a_B in terms of our fundamental model parameters α, $M_{\rm max}$, $M_{\rm min}$, and $\mathcal{N}_{\rm PBH}$, we first note that, by definition,

$$a_f \ = \ e^{-\mathcal{N}_{\rm PBH}} a_{\rm PBH} \ . \tag{3.21}$$

Moreover, during any cosmological epoch wherein w is constant, a and t are related by

$$\frac{a}{a_*} \ = \ \left(\frac{t}{t_*}\right)^{2/(3+3w)} . \tag{3.22}$$

Thus, given Eqs. (2.9) and Eqs. (2.11) we have

$$a_{\rm PBH} \ = \ \left(\frac{M_{\rm min}}{M_{\rm max}}\right)^{2/(1+\overline{w})} a_s \ . \tag{3.23}$$

Finally, since $w = 1/3$ between the end of stasis and the time of matter-radiation equality, we have

$$a_s \ = \ \left[\frac{\rho_{\rm crit}(t_{\rm MRE})}{\rho_{\rm crit}(t_s)}\right]^{1/4} a_{\rm MRE} \ , \tag{3.24}$$

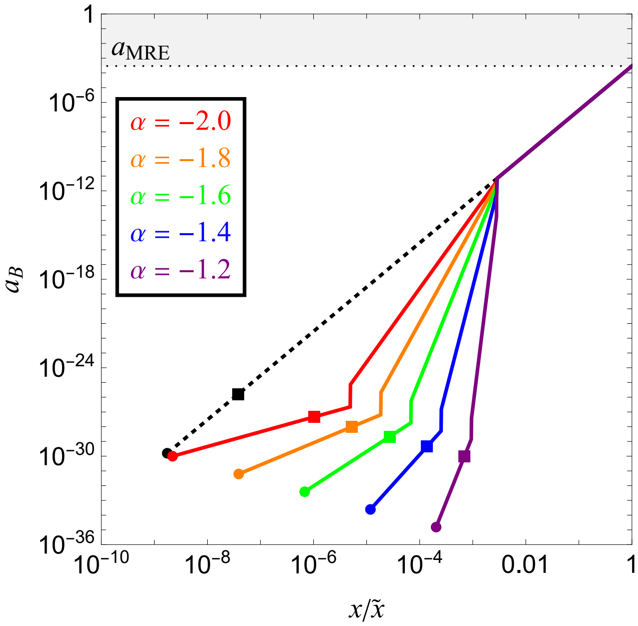

Fig. 2. The scale factor a_B at the time at which a pair of PBHs decouple from the Hubble flow and form a binary in a cosmology involving an epoch of PBH-induced stasis, shown for different values of α (solid colored curves). All of the results shown correspond to the parameter choices $M_{\rm min} = 10$ g, $M_{\rm max} = 10^9$ g, and $\mathcal{N}_{\rm PBH} = 5$. The black dashed curve indicates the corresponding result for a_B in the standard cosmology. The circular dot at the end of each curve indicates the minimum value of $x/\widetilde{x}$ for a binary with $M_B = 2M_{\rm min}$, given that a binary cannot form before its constituent PBHs are produced via gravitational collapse. The square that appears further to the right along each curve indicates the corresponding minimum value of $x/\widetilde{x}$ for a binary with $M_B = 2M_{\rm max}$.

where $a_{\rm MRE} = (1 + z_{\rm MRE})^{-1}$, with $z_{\rm MRE} \approx 3402$ [38]. Since the energy density at the end of the stasis epoch is

$$\rho_{\rm crit}(t_s) \;=\; \frac{3H^2(t_s)}{8\pi G} \;=\; \frac{3\epsilon^2 M_P^{10}}{2\pi(1+\overline{w})^2 M_{\rm max}^6} \;, \qquad (3.25)$$

the expression in Eq. (3.24) simplifies to

$$a_s \;=\; \left[\frac{2\pi(1+\overline{w})^2 \rho_{\rm MRE} M_{\rm max}^6}{3\epsilon^2 M_P^{10}}\right]^{1/4} a_{\rm MRE} \;. \qquad (3.26)$$

In a flat, ΛCDM universe, the critical density at matter-radiation equality is

$$\rho_{\rm MRE} \;=\; \frac{3H_{\rm now}^2 M_P^2}{8\pi}\Big[\Omega_{\Lambda,{\rm now}} + \Omega_{M,{\rm now}} a_{\rm MRE}^{-3} + \Omega_{\gamma,{\rm now}} a_{\rm MRE}^{-4}\Big]^{1/2} \;, \qquad (3.27)$$

where $H_{\rm now} \equiv H(t_{\rm now}) \approx 1.437 \times 10^{-42}$ GeV and where $\Omega_{M,{\rm now}} \approx 0.315$, $\Omega_{\gamma,{\rm now}} \approx 5.38 \times 10^{-5}$, and $\Omega_{\Lambda,{\rm now}} \approx 0.685$ denote the present-day abundances of matter, radiation, and vacuum energy, respectively [38].

In Fig. 2, we plot a_B as a function of $x/\widetilde{x}$ within our PBH-induced stasis cosmology for a variety of different values of α (solid colored curves). All of the results shown in the figure correspond to the parameter choices $M_{\rm min} = 10$ g, $M_{\rm max} = 10^9$ g, and $\mathcal{N}_{\rm PBH} = 5$. The black dotted curve indicates the corresponding result for a_B in the standard cosmology. The circular dot at the end of each curve indicates the minimum value of $x/\widetilde{x}$ for a binary with $M_B = 2M_{\rm min}$, given that a binary cannot form before its constituent PBHs are produced. The square that appears further to the right along each curve indicates the corresponding minimum value of $x/\widetilde{x}$ for a binary with $M_B = 2M_{\rm max}$.

We observe from Fig. 2 that the value of a_B for a pair of PBHs with a given initial comoving separation x in our PBH-induced stasis scenario is less than or equal to the corresponding result in the standard cosmology for all cases shown. This reflects the fact that $\rho_{\rm crit}$ decreases more rapidly with a during a radiation-dominated epoch than it does during a stasis epoch with $0 < \overline{w} < 1/3$ or a PBH-dominated epoch with $w = 0$. However, we note that while it is typically the case that a pair of PBHs with a given value of x decouple from the Hubble flow at an equal or smaller value of a within our stasis cosmology than they would within the standard cosmology, there are exceptions to this general rule. In particular, within the regime in which $\alpha < -3/2$, we have $w_c > 1/3$, which implies that $\rho_{\rm crit}$ decreases more slowly during a radiation-dominated epoch than it does during the PBH-formation epoch. As a result, within regions of model-parameter space in which $\alpha < -3/2$ and $\mathcal{N}_{\rm PBH}$ is small, very light black holes which are produced quite nearby each other can in fact form binaries slightly earlier within our stasis cosmology than they would within the standard cosmology. Of course, it is also the case that PBHs which decouple after stasis ends, with comoving separations such that $x/\widetilde{x} > Q_s$, decouple at the same value of a_B as they do in the standard cosmology.

IV. COALESCENCE

After they decouple from the Hubble flow, a pair of isolated PBHs which are initially at rest in the background frame will continue to travel along a straight-line path toward each other until they collide. However, the presence of additional PBHs in the vicinity will disrupt the infall of those two PBHs, which will therefore typically form a binary instead of colliding head-on. Once such a binary forms, the two constituent PBHs lose energy via the emission of gravitational radiation and merge into a single black hole. The properties of this binary — and in particular its semi-major axis r_a and semi-minor axis r_b depend on the spatial distribution of nearby PBHs.

For simplicity, following Refs. [39, 40], we approximate the formation of these binaries as a three-body process wherein the orbital properties of the binary are determined by the gravitational influence of the single additional PBH with the smallest comoving distance y from the center of mass of the two PBHs which form the binary. Refinements which account for the effect of additional PBHs were considered in [41]. In this approximation, the time that it takes for the merger of two PBHs with individual masses M_1 and M_2 whose infall is disrupted by a third PBH of mass M_3 to occur is [42]

$$\tau_m(M_1, M_2, M_3, x, y) \approx \frac{3}{85}\frac{r_a^{-3}(x) r_b^7(x,y)}{G^3 M_1 M_2 (M_1+M_2)} . \tag{4.1}$$

The semi-major axis of the orbit turns out to be proportional to the initial physical distance $r_B = a_B x$ between the two PBHs in the binary at the time at which the system initially decouples from the Hubble flow, while the semi-minor axis is proportional to the product of the tidal force and the square of the free-fall time. In particular, one finds that

$$\begin{aligned} r_a(M_1, M_2, x) &\approx \zeta_a a_B x \\ r_b(M_1, M_2, M_3, x, y) &\approx \frac{2\zeta_b M_3 r_a(x)}{(M_1+M_2)}\left(\frac{x}{y}\right)^3 , \end{aligned} \tag{4.2}$$

where ζ_a and ζ_b are proportionality factors of order unity. For the case in which $M_1 = M_2$, a detailed analysis yields the values $\zeta_a \approx 0.4$ and $\zeta_b = 0.8$ for these proportionality factors [40, 41], though merger rates obtained in this case are not particularly sensitive to the precise values of ζ_a and ζ_b [43]. Thus, while the values of ζ_a and ζ_b appropriate for a binary in which $M_1 \neq M_2$ may differ from those appropriate for a binary in which $M_1 = M_2$, such differences will not have a drastic impact on our estimate for the merger rate. Thus, following Ref. [37], we take $\zeta_a = \zeta_b = 1$.

On average, the differential number of PBHs at time t per unit PBH mass per unit comoving radial distance which are located within a spherical shell of comoving radius x centered on a particular PBH of mass M' can be expressed as

$$\frac{\partial^2 N(M, M', x)}{\partial M \partial x} = 4\pi x^2 a^3 f_{\rm BH}(M)\big[1+\xi(M, M', x)\big] , \tag{4.3}$$

where $\xi(M, M', x)$ is the two-point correlation function for the PBHs. While both $\partial^2 N(M, M', x)/\partial M \partial x$ itself and $f_{\rm BH}(M)$ depend non-trivially on t, we have suppressed the time-dependence of both quantities in this equation in order to reduce notational clutter.

The functional form of the two-point correlation function $\xi(M, M', x)$ depends on the properties of the primordial density perturbations which collapse to produce the PBHs. This correlation function may, in general, depend on both M and M'. For simplicity, we shall henceforth assume that spatial fluctuation in the primordial energy density are described by a Gaussian random field, in which case the spatial distribution of PBHs follows a Poisson distribution. For a perfectly spatially homogeneous, Poisson-distributed population of PBHs, $\xi(M, M', x) = 0$ for all x, regardless of the value of M. However, for more realistic distributions which depart from these idealized properties, a number of additional effects give rise to a non-trivial dependence of $\xi(M, M', x)$ on x. For the case of a monochromatic PBH mass spectrum, for example, it does not make sense for more than one PBH to form from gravitational collapse within the same horizon volume. Thus, for comoving separations $x < x_p(M, M')$, it follows that $\xi(M, M', x) = 0$ [44, 45]. For the case of an extended mass spectrum, the situation is more complicated, given that in this case lighter PBHs can form within regions of space which later collapse to form heavier PBHs. Nevertheless, it has been shown that the same qualitative behavior is obtained in this case [46]. Following Ref. [37], we approximate $\xi(M, M', x)$ as being independent of x for $x > x_p(M, M')$ and take

$$1+\xi(M, M', x) \approx \delta_{\rm BH}\Theta\big(x - x_p(M, M')\big) , \tag{4.4}$$

where $\delta_{\rm BH}$ is a constant and where $\Theta(x)$ denotes the Heaviside function of x.

It follows from Eq. (4.3) that the total number of PBHs of any mass located within a spherical comoving volume of radius y centered on a PBH of mass M' is

$$N(M', y) \equiv \int_0^y dx \int_0^\infty dM \, \frac{\partial^2 N(M, M', x)}{\partial M \partial x} . \tag{4.5}$$

The upper limit of integration in the integral over x is properly y rather than $\max\{y, \widetilde{x}\}$ because $N(M', y)$ represents the number of PBHs within this spherical comoving volume, not the number of binaries.

The statistical properties of three-body configurations of PBHs may be expressed in terms of the quantities defined in Eqs. (4.3) and (4.5). For example, we show in Appendix A that the joint probability density $\mathcal{P}_{\rm n,nN}(M_1, M_2, M_3, x, y)$ that the nearest neighbor of a particular PBH of mass M_1 will be located a comoving distance x away from that first PBH, that the next-to-nearest neighbor of that same PBH will be located a distance y away from that first PBH, and that these two PBHs will have masses M_2 and M_3, respectively, takes the form

$$\begin{aligned} &\mathcal{P}_{\rm n,nN}(M_1, M_2, M_3, x, y) = \\ &\qquad e^{-N(M_1, y)} \frac{\partial^2 N(M_2, M_1, x)}{\partial M_2 \partial x} \frac{\partial^2 N(M_3, M_1, y)}{\partial M_3 \partial y} . \end{aligned} \tag{4.6}$$

We note that this joint probability density is independent of M_1. The corresponding differential comoving number density $\widetilde{n}(M_1, M_2, M_3, x, y)$ of PBH nearest-neighbor pairs in which one PBH has mass M_1 and its nearest and next-to-nearest neighbor have these attributes is

$$\begin{aligned} \widetilde{n}(M_1, M_2, M_3, x, y) &= \frac{1}{2} a^3 f_{\rm BH}(M_1) \\ &\quad \times \mathcal{P}_{\rm n,nN}(M_1, M_2, M_3, x, y) , \end{aligned} \tag{4.7}$$

where the factor of $1/2$ accounts for the fact that there are two PBHs per binary and thus compensates for a double-counting.

Integrating the expression in Eq. (4.7) over x and y while imposing the condition that the total time $\tau_m(M_1, M_2, M_3, x, y) + t_B(M_1, M_2, x)$ that it takes for a pair of PBHs to form a binary and then coalesce be equal to t, we obtain

$$\mathcal{R}_3(M_1, M_2, M_3) = \int_0^{\widetilde{x}} dx \int_x^{\infty} dy \Big[\widetilde{n}(M_1, M_2, M_3, x, y) \times \delta\big(t - \tau_m(M_1, M_2, M_3, x, y) - t_B(M_1, M_2, x)\big)\Big] , \tag{4.8}$$

where the upper limit of integration in the integral over x is properly $\widetilde{x}$ because PBH binaries do not form after matter-radiation equality. We shall henceforth refer to $\mathcal{R}_3(M_1, M_2, M_3)$ as the differential three-body merger rate. Physically, it represents the differential contribution per comoving volume per unit M_1, M_2, and M_3 to the rate at which the differential comoving number density of PBH nearest-neighbor pairs with masses M_1 and M_2 whose next-to-nearest neighbor has mass M_3 decreases with t due to binary mergers. The quantity which is typically referred to in the literature as the differential PBH merger rate — and to which we shall here refer as the differential two-body merger rate — may be obtained simply by integrating this expression over all possible values for the mass of that next-to-nearest neighbor:

$$\mathcal{R}_2(M_1, M_2) \equiv \int_0^{\infty} dM_3 \, \mathcal{R}_3(M_1, M_2, M_3) . \tag{4.9}$$

The differential two-body merger rate gives rise to both the source and sink terms for $f_{\rm BH}(M)$ which appear in Eq. (2.1). Indeed, both $\Gamma_+(M, t)$ and $\Gamma_-(M, t)$ can be obtained from $\mathcal{R}(M_1, M_2)$ by direct integration. In particular, these PBH production and destruction rates are given by

$$\begin{aligned}\Gamma_+(M) &= \frac{1}{a^3 f_{\rm BH}(M)} \int_0^{\infty} dM_1 \int_0^{\infty} dM_2 \Big[\mathcal{R}_2(M_1, M_2) \times \delta(M - M_1 - M_2)\Big] \\ \Gamma_-(M) &= \frac{1}{a^3 f_{\rm BH}(M)} \int_0^{\infty} dM_2 \mathcal{R}_2(M, M_2) ,\end{aligned} \tag{4.10}$$

where we have suppressed the explicit time-dependence in $\Gamma_\pm(x, t)$ in order to avoid notational clutter.

V. PBH MERGERS: RESULTS

Our primary goal is to determine the region of parameter space within which $\Gamma_-(M, t)$ and $\Gamma_+(M, t)$ both remain sufficiently small until the end of the stasis epoch that the effect of mergers can be neglected. Within this region, presuming for the moment that the effect of accretion can likewise be neglected, $f_{\rm BH}(M, t)$ evolves only as a consequence of evaporation and cosmological redshifting. Indeed, if either of the conditions $\Gamma_+(M, t) \ll H$ and $\Gamma_+(M, t) \ll H$ is violated at any time t within the range $t_i < t < \tau_e(M_{\rm max})$ for any M within the range $M_{\rm min} \leq M \leq M_{\rm max}$, then the shape of $f_{\rm BH}(M, t)$ evolves non-trivially at all subsequent times and the dynamics which give rise to stasis are disturbed prior to the time at which the stasis epoch would otherwise have ended.

It is important to note, however, that even in situations in which these conditions are not satisfied for all M within the range $M_{\rm min} \leq M \leq M_{\rm max}$, a stasis epoch is not necessarily precluded; rather, it may simply be abridged. Mergers which involve a PBH of mass M' can only affect the portion of $f_{\rm BH}(M, t)$ for which $M \geq M'$. Moreover, since all of the PBHs are non-relativistic objects which behave like massive matter, mergers in and of themselves have no effect on the manner in which $\rho_{\rm BH}$ evolves with time. Indeed, the only way in which mergers affect the expansion history is by altering the spectrum of evaporation times $\tau_e(M)$ for the population of PBHs. However, since PBHs with larger masses evaporate later, mergers which involve a PBH of mass M can only affect the expansion history at times $t \geq t_e(M)$. Taken together, these observations imply that if M_D is the lowest value of M for which the conditions $\Gamma_+(M, t) \ll H$ and $\Gamma_-(M, t) \ll H$ are ever violated while $t_i < t < \tau_e(M_{\rm max})$, then distortions of $f_{\rm BH}(M, t)$ caused by mergers only begin to affect the stasis dynamics at times $t > \tau_e(M_D)$. Thus, a population of PBHs with an initial mass spectrum of the form in Eq. (2.5) still gives rise to a stasis epoch, but one which ends at $t = \tau_e(M_D)$ rather than $t = \tau_e(M_{\rm max})$. This stasis epoch is then followed by a transition period similar to that which arises in stasis scenarios involving towers of decaying particles [16], wherein the effective equation-of-state parameter w for the universe varies non-trivially with time. This transition period ends once the heaviest PBHs ultimately generated by mergers evaporate completely, at which point the universe becomes radiation-dominated and remains so until $t_{\rm MRE}$.

For the purposes of identifying the region of our parameter space within which the effect of mergers on stasis are negligible and determining the value of M_D for points which lie outside of this region, it is not necessary for us to determine precisely *how* $f_{\rm BH}(M, t)$ behaves once either of the conditions $\Gamma_+(M, t) \ll H$ or $\Gamma_-(M, t) \ll H$ is violated, but merely to determine *whether* and *when* that condition is violated. Thus, proceeding in accord with the assumption that the effect of accretion is also negligible — an assumption which, as we shall see in Sect. VI, holds throughout the majority of our parameter-space region of interest — we may proceed by evaluating $\Gamma_+(M, t)$ and $\Gamma_-(M, t)$ as functions of M and t for the simple form of $f_{\rm BH}(M, t)$ which is obtained when only expansion and evaporation are important.

This form of $f_{\rm BH}(M, t)$ may be inferred from the observation that when only these two processes have a non-negligible impact on the differential number density, the comoving number density of PBHs with initial masses in the infinitesimal range from M_i to $M_i + dM_i$ remains constant until these PBHs evaporate. This implies that

$$f_{\rm BH}(M,t)dM \;\approx\; \frac{a_i^3}{a^3} f_{\rm BH}(M_i,t_i)\Theta\Big(\tau_e(M_i)-(t-t_i)\Big)dM_i \;, \tag{5.1}$$

where $a_i \equiv a(t_i)$. Since $M(t) \approx M_i\Theta(\tau_e(M_i)-(t-t_i))$ in the instantaneous-evaporation approximation, it then follows that within this region of parameter space, $f_{\rm BH}(M,t)$ is approximately given by

$$\begin{aligned} f_{\rm BH}(M,t) \;&\approx\; \frac{(\alpha+1)\rho_{{\rm BH},i}M^{\alpha-1}a_i^3}{(M_{\rm max}^{\alpha+1}-M_{\rm min}^{\alpha+1})a^3}\Theta\big(M-M_{\rm cut}(t)\big) \\ &\quad \times \Theta(M_{\rm max}-M) \;, \end{aligned} \tag{5.2}$$

where $M_{\rm cut}(t) \equiv \max\{M_{\rm min}, \widetilde{M}(t)\}$ is the mass of the lightest PBH in the spectrum at time t and where

$$\widetilde{M}(t) \;\equiv\; \left[3\epsilon M_P^4(t-t_i)\right]^{1/3}$$

denotes the initial mass of the PBH whose evaporation time is $\tau_e(M_i) = t$.

For such a form of $f_{\rm BH}(M,t)$, the quantity defined in Eq. (4.3) reduces to

$$\begin{aligned} \frac{\partial^2 N(M,M',x)}{\partial M\partial x} \;&=\; \frac{3\,\mathcal{C}_N x^2 M^{\alpha-1}}{M_P^{\alpha-3}}\Theta\big(x-x_p(M,M')\big) \\ &\quad \times \Theta(M_{\rm max}-M)\Theta\big(M-M_{\rm cut}(t)\big) \;, \end{aligned} \tag{5.3}$$

where we have defined the dimensionless coefficient

$$\mathcal{C}_N \;\equiv\; \frac{4\pi M_P^{\alpha-3}\rho_{{\rm BH},i}(\alpha+1)\delta_{\rm BH}a_i^3}{3(M_{\rm max}^{\alpha+1}-M_{\rm min}^{\alpha+1})} \;. \tag{5.4}$$

Integrating this result over x and M, we obtain

$$\begin{aligned} N(M',y) \;&=\; \frac{\mathcal{C}_N}{M_P^{\alpha-3}}\int_{M_{\rm cut}(t)}^{M_{\rm max}} dM\,M^{\alpha-1}\left[y^3-x_p^3(M,M')\right] \\ &\quad \times \Theta\big(y-x_p(M,M')\big) \;. \end{aligned} \tag{5.5}$$

Given the expression for $x_p(M,M')$ in Eq. (3.15), we observe that the Heaviside function appearing in this expression for $N(M',y)$ is equivalent to

$$\Theta\big(y-x_p(M,M')\big) \;=\; \Theta\big(M_*(y)-M\big)\Theta\big(M_*(y)-M'\big) \;,$$

where have defined $M_*(y) \equiv M_P(y/\hat{x})^{-3/\alpha}$. Thus, integrating over M, we find that until the time at which $\widetilde{M}(t) = M_{\rm max}$ and the entire population of PBHs has evaporated, our expression for $N(M',y)$ evaluates to

$$\begin{aligned} N(M',y) \;&=\; \frac{\mathcal{C}_N\hat{x}^3M_P^3}{\alpha}\left[\frac{M_\uparrow^\alpha(y)-M_{\rm cut}^\alpha}{M_*^\alpha(y)} - \log\left(\frac{M_\uparrow^\alpha(y)}{M'^\alpha}\right)\right. \\ &\quad \left. + \left(\frac{M_{\rm cut}}{M'}\right)^\alpha - 1\right]\Theta\big(M_*(y)-M'\big) \;, \end{aligned} \tag{5.6}$$

where we have defined $M_\uparrow \equiv \min\{M_{\rm max}, M_*(y)\}$.

While the parametric dependence of $N(M',y)$ on y is perhaps not immediately transparent from Eq. (5.6), it is not difficult to show that this quantity, which represents the number of PBHs within a spherical comoving volume of radius y, scales with y in a manner which accords with this physical interpretation. Indeed, we note that the contribution from the first term within the square brackets on the right side of this equation typically dominates over the contribution from the remaining terms. Thus, roughly speaking, $N(M',y)$ scales with y as

$$N(M',y) \;\sim\; \begin{cases} \dfrac{M_{\rm cut}^\alpha}{M_*^\alpha(y)}\left(1-\dfrac{M_{\rm max}^\alpha}{M_{\rm cut}^\alpha}\right) & M_*(y) > M_{\rm max} \\ \dfrac{M_{\rm cut}^\alpha}{M_*^\alpha(y)} - 1 & M_*(y) < M_{\rm max} \end{cases} \tag{5.7}$$

at times $t \le t_s$. Regardless of the relationship between $M_*(y)$ and $M_{\rm max}$, this implies that $N(M',y)$ is a monotonically increasing function of y. Moreover, Eq. (5.7) also implies that within the regime in which y is sufficiently large that $M_*(y) \gg M_{\rm cut}(t)$, we may approximate $N(M',t)$ as

$$N(M',t) \;\approx\; B_N(t)y^3 \;, \tag{5.8}$$

where the y-independent prefactor $B_N(t)$ in this expression scales differently with t during different cosmological epochs. Prior to the beginning of the stasis epoch, $M_{\rm cut} = M_{\rm min}$ and $B_N(t)$ is therefore independent of t. By contrast, during the stasis epoch, $M_{\rm cut} = M_{\rm max}(t/t_s)^{1/3}$ and $B_N(t)$ scales with t as

$$B_N(t) \;\sim\; \begin{cases} t^{\alpha/3}\left[1-(t/t_s)^{-\alpha/3}\right] & M_*(y) > M_{\rm max} \\ t^{\alpha/3} & M_*(y) < M_{\rm max} \;. \end{cases} \tag{5.9}$$

Regardless of the relationship between $M_*(y)$ and $M_{\rm max}$, this is well approximated by $B_N(t) \sim t^{\alpha/3}$ until the universe approaches the end of stasis. Finally, for $t > t_s$, the entire population of PBHs has already evaporated, so $B_N(t) = 0$. Physically, Eq. (5.8) indicates that within the regime in which y is large, $N(M',y)$ is proportional to the volume of a comoving sphere of radius y, as expected.

Given the result in Eqs. (5.6), we are now equipped to evaluate $\mathcal{R}_3(M_1,M_2,M_3)$ in our PBH-induced stasis scenario. Since $\tau_m(M_1,M_2,M_3,x,y)$ is a monotonically decreasing function of y, we find that the Dirac δ-function appearing in Eq. (4.8) may be expressed as

$$\begin{aligned} \delta\big(t-\tau_m(x,y)-t_B(x)\big) \;&=\; \frac{y\delta\big(y-y_B(x,t)\big)}{21\tau_m(x,y)} \\ &=\; \frac{y_B(x,t)}{21[t-t_B(x)]}\,\delta\big(y-y_B(x,t)\big) \\ &\quad \times \Theta\big(t-t_B(x)\big) \;, \end{aligned} \tag{5.10}$$

where the Heaviside function is needed to ensure that only contributions from binaries which have formed by time t contribute to the merger rate and where we have defined

$$y_B(x,t) \;\equiv\; x_B(t)\left[\frac{x^{25}a_B^4(x)}{\widetilde{x}^{25}a_{\rm MRE}^4}\right]^{1/21} \tag{5.11}$$

in terms of the quantity

$$x_B(t) \;\equiv\; \left[\frac{384}{85}\frac{M_P^6 M_3^7\zeta_a^4\zeta_b^7 a_{\rm MRE}^4\widetilde{x}^{25}}{M_1M_2(M_1+M_2)^8(t-t_B)}\right]^{1/21}~. \tag{5.12}$$

We note that $x_B(t)$ depends on t but not on x. Since the expression for $a_B(x)$ in Eq. (3.8) is a piecewise function of x, the quantity $y_B(x,t)$ is likewise a piecewise function of x. Explicitly, we find that

$$y_B(x,t) \;=\; \begin{cases} x_B\left(\dfrac{x}{\widetilde{x}}\right)^{37/21} & 1>\dfrac{x}{\widetilde{x}}>Q_s \\ x_B\left[\dfrac{a_{\rm PBH}}{a_{\rm MRE}Q_{\rm PBH}^{1/\overline{w}}}\right]^{\frac{4}{21}}\left(\dfrac{x}{\widetilde{x}}\right)^{\frac{25+4/\overline{w}}{21}} & Q_s>\dfrac{x}{\widetilde{x}}>Q_{\rm PBH} \\ x_B\left[\dfrac{a_{\rm PBH}}{a_{\rm MRE}}\right]^{\frac{4}{21}}\left(\dfrac{x}{\widetilde{x}}\right)^{\frac{25}{21}} & Q_{\rm PBH}>\dfrac{x}{\widetilde{x}}>Q_f \\ x_B\left[\dfrac{a_f}{a_{\rm MRE}Q_f^{1/w_c}}\right]^{\frac{4}{21}}\left(\dfrac{x}{\widetilde{x}}\right)^{\frac{25+4/w_c}{21}} & Q_f>\dfrac{x}{\widetilde{x}}~. \end{cases} \tag{5.13}$$

While this expression is somewhat complicated, the manner in which y_B scales with x, on t, and the masses M_1, M_2, and M_3 is in fact relatively straightforward. Since it is almost always the case that $\tau_m(M_1,M_2,M_3,x,y)\gg t_B(M_1,M_2,x)$ for the binary configurations which collectively dominate the merger rate a given time t, one can typically approximate $t-t_B\approx t$ in Eq. (5.12). In this approximation, we have

$$y_B(x,t) \;=\; A_B(t)\,x^{(25+\beta)/21}~, \tag{5.14}$$

where the value of β and the manner in which the x-independent prefactor $A_B(t)$ scales with M_1, M_2, M_3, and t both depend on the value of w during that epoch. In particular,

$$\beta \;=\; \begin{cases} 4/w & w\;>\;0 \\ 0 & w\;=\;0~, \end{cases} \tag{5.15}$$

while $A_B(t)$ scales with these quantities as

$$A_B(t) \;\sim\; \frac{M_3^{1/3}}{(M_1M_2\,t)^{1/21}(M_1+M_2)^{(24+\beta)/63}}~. \tag{5.16}$$

As we shall see, this scaling behavior plays a crucial role in determining how $\Gamma_+(M,t)$ and $\Gamma_-(M,t)$ depend on M and t for any given choice of model parameters.

Given these results, we find that the general expression for $\mathcal{R}_3(M_1,M_2,M_3)$ in Eq. (4.8) simplifies in the context of our PBH-induced stasis scenario to

$$\begin{aligned}\mathcal{R}_3(M_1,M_2,M_3) \;=\; & \frac{8\pi^2\delta_{\rm BH}^2}{21}\left[\prod_{j=1}^{3}a^3 f_{\rm BH}(M_j)\right] \\ & \times\int_{\min\{x_F,\,x_p(M_1,M_2)\}}^{x_F}dx\,\Bigg[\mathcal{I}(x)\Theta\big(y_B(x)-x\big) \\ & \times\Theta\big(y_B(x)-x_p(M_1,M_3)\big)\Bigg]~,\end{aligned} \tag{5.17}$$

where we have once again suppressed the explicit time-dependence in quantities such as $y_B(x,t)$ and $f_{\rm BH}(M,t)$ in order to avoid notational clutter and where, for future reference, we have defined

$$\mathcal{I}(x) \;\equiv\; \frac{x^2y_B^3(x)}{t-t_B}e^{-N(M_1,y_B(x))}~. \tag{5.18}$$

The upper limit of integration x_F in Eq. (5.17) follows from the Heaviside function in Eq. (5.10), which we can rewrite as a function of x by inverting the relation between x and t_B in Eq. (3.11). Given that the decoupling time for binaries with $Q_f<x/\widetilde{x}<Q_{\rm PBH}$ is $t_{\rm PBH}$, we have

$$x_F(t) \;\equiv\; \begin{cases} \widetilde{x}\left(\dfrac{t}{t_{\rm MRE}}\right)^{1/6} & t_s<t<t_{\rm MRE} \\ \widetilde{x}\,Q_{\rm PBH}\left(\dfrac{t}{t_{\rm PBH}}\right)^{\frac{2\overline{w}}{3(1+\overline{w})}} & t_{\rm PBH}<t<t_s \\ \widetilde{x}\,Q_f & t_f<t<t_{\rm PBH} \\ \widetilde{x}\,Q_f\left(\dfrac{t}{t_f}\right)^{\frac{2w_c}{3(1+w_c)}} & t_i<t<t_f~. \end{cases} \tag{5.19}$$

We note that $x_F\leq\widetilde{x}$ for all $t_i<t<t_{\rm MRE}$, and thus the upper bound $x<x_F$ is more restrictive than the bound $x<\widetilde{x}$ in all cases. We also note that since the comoving quantity $a^3f_{\rm BH}(M_j)$ is time-independent at times $t\lesssim\tau_e(M_j)$ within any region of parameter space within which the effect of mergers and accretion is negligible, $\mathcal{R}_3(M_1,M_2,M_3)$ depends on t entirely through $\mathcal{I}(x)$, through $x_F(t)$, and through the Heaviside functions.

The explicit lower limit of integration in the integral over x in Eq. (5.17) accounts for fact that this integral vanishes for combinations of M_1 and M_2 which yield $x_p(M_1,M_2)>x_F$. However, it is the additional, implicit thresholds imposed by the Heaviside functions appearing in the integrand which typically determine the lower limit of integration. As we shall see, these thresholds play a central role in determining not only how $\mathcal{R}_3(M_1,M_2,M_3)$ depends on M_1, M_2, and M_3, but also how this differential three-body merger rate evolves with t for any particular combination of these masses.

The expressions for the rates $\Gamma_+(M)$ and $\Gamma_-(M)$ which follow from this form of $\mathcal{R}_3(M_1,M_2,M_3)$ can be obtained via numerical integration. However, in order to provide physical motivation for the results we obtain in this way, we first pause to examine in greater detail how the expression for $\mathcal{R}_3(M_1, M_2, M_3)$ in Eq. (5.17) depends on the individual masses M_1, M_2, and M_3. Our first step in this direction shall be to define

$$\Gamma_3(M_1, M_2, M_3) \;\equiv\; \frac{M_2 M_3 \mathcal{R}_3(M_1, M_2, M_3)}{a^3 f_{\rm BH}(M_1)} \;. \tag{5.20}$$

The additional factors present in $\Gamma_3(M_1, M_2, M_3)$ relative to $\mathcal{R}_3(M_1, M_2, M_3)$ have been included such that

$$\Gamma_3(M_1, M_2, M_3) \;=\; \frac{\partial^2 \Gamma_-(M_1)}{\partial \log M_2 \partial \log M_3} \;. \tag{5.21}$$

In Fig. 3 we display a series of density plots which together illustrate how $\Gamma_3(M_1, M_2, M_3)$ evolves over time. Each of the four panels of this figure represents a "snapshot" of this quantity, normalized to the value $H_{\rm PBH} = H(t_{\rm PBH})$ of the Hubble expansion rate at the beginning of the stasis epoch, in the (M_2, M_3)-plane at a different time between t_i and t_s for a population of PBHs characterized by parameter choices $M_{\rm min} = 1$ g, $M_{\rm max} = 10^5$ g, $\mathcal{N}_{\rm PBH} = 2$, and $\alpha = -2$ and for $M_1 = 10^5$ g. The results shown in the top left panel correspond to a time during the PBH-formation epoch, those in the top right panel correspond to a time shortly after the PBH-domination epoch has concluded, and those in the bottom two panels correspond to later times during the stasis epoch. Within the gray region shown in each panel, either M_2 or M_3 lies below $M_{\rm cut}(t)$ at the corresponding time t. This implies that at least one of the PBHs would already have evaporated, so no configuration of PBHs with such a combination of masses exists at that time.

The results shown within each individual panel of Fig. 3 provide a sense of how $\Gamma_3(M_1, M_2, M_3)$ varies with M_2 and M_3. Within each panel, we observe that $\Gamma_3(M_1, M_2, M_3)$ decreases monotonically as M_2 increases, indicating that mergers between a heavy PBH and a very light PBH are far more common than mergers between two heavy PBHs. By contrast, the manner in which $\Gamma_3(M_1, M_2, M_3)$ depends on M_3 is more complicated. In all but the lower right panel of the figure, $\Gamma_3(M_1, M_2, M_3)$ rises, peaks, and then falls as M_3 increases from $M_{\rm cut}(t)$ to $M_{\rm max}$. In fact, as we shall see, the only reason this behavior is not also manifest in the bottom right panel is that the portion of the (M_2, M_3)-plane within which $\Gamma_3(M_1, M_2, M_3)$ would otherwise be observed to increase with M_3 lies within the region wherein $M_3 < M_{\rm cut}(t)$.

The origin of this non-monotonic behavior ultimately stems from an interplay between the function $\mathcal{I}(x)$ defined in Eq. (5.18) and the Heaviside functions which modify the limits of integration in the integral over x in Eq. (5.17). Since Eqs. (5.6) and (5.14) together imply that $N(M_1, y_B(x))$ is an increasing function of x, we may view $\mathcal{I}(x)$ as a function of x which exhibits power-law growth for sufficiently small x, but is suppressed at large x by an exponential cutoff. The integral in Eq. (5.17) is in general dominated by the contribution from values of x near the value $x_{\rm peak}$ at which this sharply peaked function is maximized — provided, of course, that $x_{\rm peak} \gtrsim \max\{x_p, x_{\rm thresh}\}$, where $x_{\rm thresh}$ is the threshold value of x imposed by the Heaviside functions.

The manner in which both $x_{\rm thresh}$ and $x_{\rm peak}$ scale with M_2 and M_3 is ultimately determined by the manner in which $y_B(x)$ scales with these quantities. Using the approximate form of $N(M', y)$ in Eq. (5.8) and once again approximating $t - t_B \approx t$, we find that

$$\begin{aligned} x_{\rm peak} \;&=\; \eta^{7/(25+\beta)} \left(A_B B_N^{1/3}\right)^{-21/(25+\beta)} \\ x_{\rm thresh} \;&=\; A_B^{-21/(4+\beta)} \;, \end{aligned} \tag{5.22}$$

where for convenience we have defined $\eta \equiv (39+\beta)/(25+\beta)$.

Since $B_N(t)$ is independent of both M_2 and M_3, the relationship between $x_{\rm peak}$ and $x_{\rm thresh}$ within any individual panel of Fig. 3 is determined entirely by $A_B(t)$. Eq. (5.16) implies that both $x_{\rm peak}$ and $x_{\rm thresh}$ increase as M_2 increases, but decrease as M_3 increases. However, $x_{\rm thresh}$ is more sensitive to changes in both of these masses. Thus, for a given value of t, it is often the case that $x_{\rm peak} < x_{\rm thresh}$ within some regions of the (M_2, M_3)-plane, while $x_{\rm peak} > x_{\rm thresh}$ within other regions.

By contrast, we note that x_p — which, like $x_{\rm thresh}$ provides an upper bound on the lower limit of integration in Eq. (5.17) — is completely independent of M_3 and is likewise effectively independent of M_2 within the regime in which $M_2 \ll M_1$. Within the regime in which $M_2 \gtrsim M_1$, however, x_p increases as M_2 increases.

Finally, we note that the value of $\mathcal{I}(x)$ at $x = x_{\rm peak}$ is

$$\mathcal{I}(x_{\rm peak}) \;=\; \left(\frac{e}{\eta}\right)^{-\eta} \frac{1}{t} A_B^{-3(\eta-1)} B_N^{-\eta} \;. \tag{5.23}$$

Since $\eta > 1$ for all $-2 \leq \alpha \leq -1$, it it always the case that $\mathcal{I}(x_{\rm peak})$ increases as M_2 increases, but decreases as M_3 increases.

These considerations together account for the manner in which $\Gamma_3(M_1, M_2, M_3)$ varies throughout the (M_2, M_3)-plane within each individual panel of Fig. 3. However, we focus on the results shown in the top left panel for purposes of illustration, since the region of the plane within which M_2 and M_3 both exceed $M_{\rm cut}$ is the broadest. Across the entire left edge of the panel, $x_{\rm peak} \ll x_{\rm thresh}$ and $\mathcal{I}(x)$ has negligible support within the integration region. As a result, $\Gamma_3(M_1, M_2, M_3)$ is highly suppressed. However, as M_3 increases with held M_2 fixed, $x_{\rm thresh}$ decreases more rapidly than $x_{\rm peak}$. Eventually, $x_{\rm thresh}$ decreases to the point at which it overtakes $x_{\rm peak}$ and the peak enters the integration region, leading to a dramatic increase in $\Gamma_3(M_1, M_2, M_3)$. However, $\mathcal{I}(x_{\rm peak})$ and the additional overall factor $M_3 f_{\rm PBH}(M_3)$ in $\Gamma_3(M_1, M_2, M_3)$ also both decrease as M_3 increases. Thus, as M_3 is further increased to the extent where $x_{\rm peak} \gg x_{\rm thresh}$ and the entire range of x within which $\mathcal{I}(x)$ has non-negligible sup-

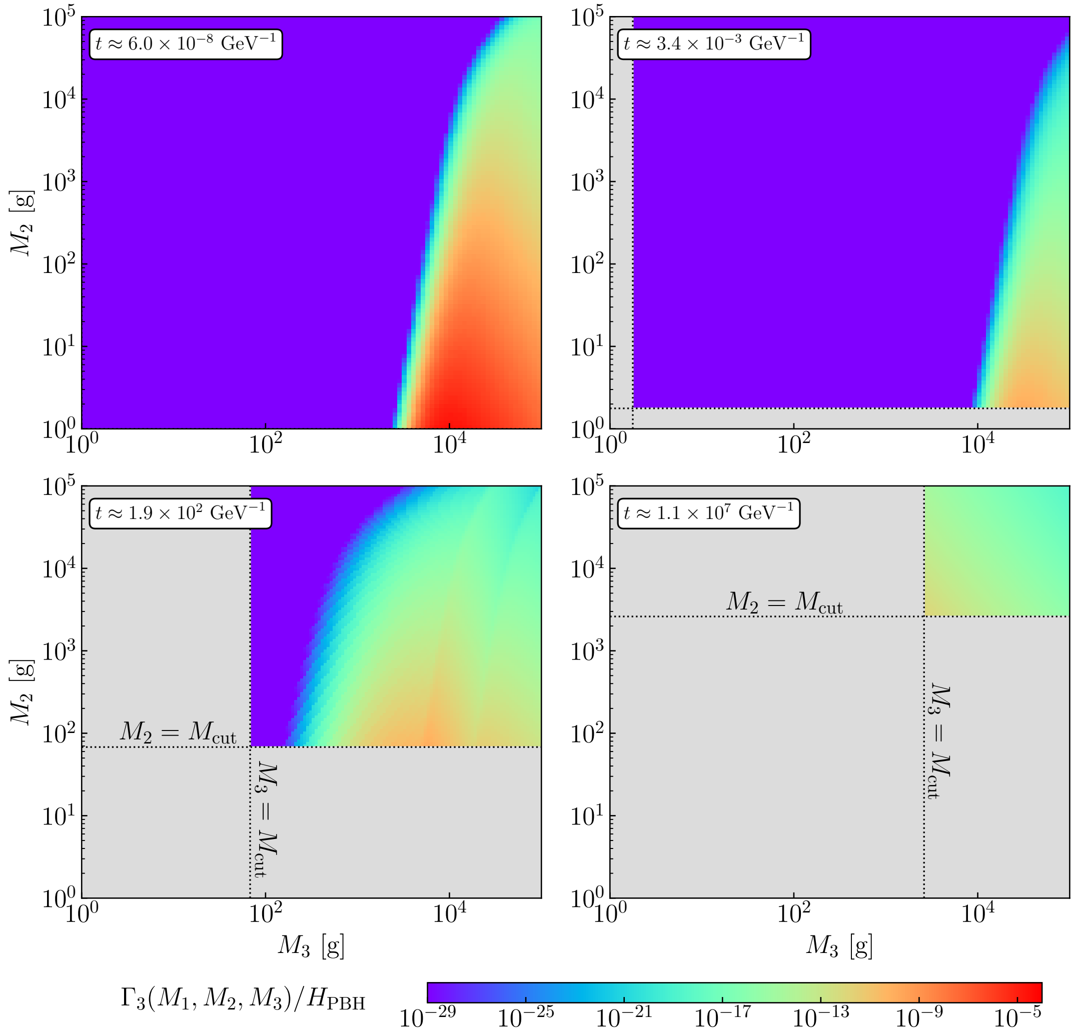

Fig. 3. The ratio $\Gamma_3(M_1, M_2, M_3)/H_{\rm PBH}$ of the differential merger rate defined in Eq. (5.20) to the value $H_{\rm PBH} = H(t_{\rm PBH})$ of the Hubble expansion rate at the beginning of the stasis epoch for the parameter choices $M_{\rm min} = 1$ g, $M_{\rm max} = 10^5$g, $\mathcal{N}_{\rm PBH} = 2$, $\alpha = -2$, and $M = 10^5$ g. Each panel is a density plot of this ratio within the (M_2, M_3)-plane evaluated at a different time t within the range $t_i < t < t_s$. The gray region of each panel indicates the region of the plane wherein either M_2 or M_3 lies below the corresponding value of $M_{\rm cut}(t)$.

port lies inside the integration region, this suppression effect eventually causes $\Gamma_3(M_1, M_2, M_3)$ to decrease.

There is a second effect which can also contribute to the decrease in $\Gamma_3(M_1, M_2, M_3)$ as M_3 increases — one whose contribution is frequently far more dramatic than that which results from the decrease in $\mathcal{I}(x_{\rm peak})$. This effect stems from the fact that x_p remains fixed as M_3 increases, which in turn implies that as M_3 increases, there is a point at which $x_{\rm thresh}$ falls below x_p. Since $x_{\rm peak}$ continues to decrease as M_3 further increases beyond this point, the range of x within which $\mathcal{I}(x)$ has significant support eventually also falls below x_p, and $\Gamma_3(M_1, M_2, M_3)$ decreases as a result. Indeed, as we shall see, this effect can have a particularly dramatic effect on the manner in which $\Gamma_3(M_1, M_2, M_3)$ varies with M_3 in situations in which α is close to -1 and that range of x is particularly narrow.

By contrast, the manner in which $\Gamma_3(M_1, M_2, M_3)$ scales with M_2 involves no such competition. As M_2 increases, not only does $x_{\rm thresh}$ rise, but the product of $\mathcal{I}(x_{\rm peak})$ and the corresponding overall factor $M_2 f_{\rm PBH}(M_2)$ in $\Gamma_3(M_1, M_2, M_3)$ actually decreases. As M_2 approaches M_1, the quantity $M_1 + M_2$ becomes sensitive to the value of M_2 and $\Gamma_3(M_1, M_2, M_3)$ begins to drop even more steeply with increasing M_2.

The manner in which $\Gamma_3(M_1, M_2, M_3)$ varies across the (M_2, M_3)-plane in the other panels of Fig. 3 exhibits the same qualitative behavior. However, as alluded to above, regions of the plane within which certain aspects of this behavior would otherwise be manifest lie within the gray region in which $M_3 < M_{\rm cut}$ at late times. Indeed, in the bottom right panel, the region of the plane within which $\Gamma_3(M_1, M_2, M_3)$ would otherwise be seen to increase with increasing M_3 lies within this gray region. Another feature which deserves comment is the set of ribbon-like streaks evident in the third panel of Fig. 3. These streaks are ultimately a consequence of the discontinuity in $a_B(x)$ which reflects from the suppression of binary capture during the PBH-dominated epoch. This discontinuity in turn gives rise to discontinuities in $y_B(x)$ and $\mathcal{I}(x)$. When $x_{\rm thresh}$ lies near one of these discontinuities in $\mathcal{I}(x)$, small changes in M_2 or M_3 can lead to large shifts in $\Gamma_3(M_1, M_2, M_3)$. The abruptness of these shifts in part reflects the standard approximations discussed above Eq. (3.4) which we have invoked in deriving an implicit expression for t_B. Indeed, the boundaries of the features which appear in the third panel of Fig. 3 would presumably appear smoother, given a more detailed treatment. However, we emphasize that whereas binary formation does not completely cease during the PBH-dominated epoch, its suppression during this epoch *is* physical, and the qualitative features in $\Gamma_3(M_1, M_2, M_3)$ to which it leads are physical as well.

Having examined how $\Gamma_3(M_1, M_2, M_3)$ depends on M_2 and M_3 for fixed t, we now consider how this quantity evolves with t for fixed M_2 and M_3. A comparison across these different panels reveals that the dependence of $\Gamma_3(M_1, M_2, M_3)$ on t is more complicated than its dependence on M_2 and M_3. This is because $x_{\rm peak}$ and $\mathcal{I}(x_{\rm peak})$ likewise scale with t in a more complicated manner. This is primarily due to the fact that $B_N(t)$ depends non-trivially on t during the stasis epoch. During the PBH-formation and PBH-dominated epochs, $B_N(t)$ is effectively constant and $x_{\rm peak}$ and $x_{\rm thresh}$ both scale with t in exactly the same way that they scale with M_2. Thus, $x_{\rm thresh}$ increases with t more rapidly than does $x_{\rm peak}$, and the region of the (M_2, M_3)-plane within which $\Gamma_3(M_1, M_2, M_3)$ is non-negligible consequently decreases. This effect accounts for the difference between the results in the top left panel of Fig. 3 (which corresponds to a time during the PBH-formation epoch) and those in the top right panel (which corresponds to a time only slightly after the stasis epoch has begun). By contrast, once stasis begins, the situation changes due to the additional time-dependence in $B_N(t)$. During stasis, $x_{\rm peak}$ actually increases *more* rapidly than $x_{\rm thresh}$. As a result, the region of the (M_2, M_3)-plane within which $x_{\rm peak} > x_{\rm thresh}$ expands over time. This accounts for the difference between the results shown in the top right and bottom left panels. Of course, as t increases during stasis, $M_{\rm cut}$ also increases, and the region of the plane within which there still exist configurations of PBHs with a given combination of M_2 and M_3 shrinks to zero as $t \to t_s$.

In Fig. 4, we show the integrated merger rates $\Gamma_+(M)$ (solid colored curves) and $\Gamma_-(M)$ (corresponding dashed curves) obtained from our expression in Eq. (5.17) for a variety of different values of M as functions of the time t. The value of the Hubble parameter (solid black curve) is also plotted alongside these curves for reference. Each panel corresponds to a different choice of α, and the results shown in all panels correspond to the parameter choices $M_{\rm min} = 1$ g, $M_{\rm max} = 10^5$ g, and $\mathcal{N}_{\rm PBH} = 2$. The range of t shown in each panel extends from t_i to t_s, and the values of t_f and $t_{\rm PBH}$ are indicated by the two vertical dashed lines. The four red dots indicated on the $M = 10^5$ g curve in the upper left panel correspond to the values of t for which $\Gamma_3(M_1, M_2, M_3)/H_{\rm PBH}$ is plotted for this M_1 value in the four panels of Fig. 3. Since it is always the case that $\Gamma_+(M_{\rm min}) = 0$ — by definition, there exist no lighter PBHs within the spectrum which could merge to form a PBH of mass $M = M_{\rm min}$ — only a dashed curve appears in any of the four panels for $M = 1$ g.

We observe from Fig. 4 that the values of $\Gamma_+(M)$ and $\Gamma_-(M)$ for any given value of M are typically quite similar in magnitude and evolve in a similar manner throughout the range of t shown. The only exceptions are cases in which M lies very near $M_{\rm max}$. We also observe that, broadly speaking, $\Gamma_+(M)$ and $\Gamma_-(M)$ both decrease over time as the universe evolves from t_i to t_s. At early times, this decrease is primarily due to the phenomenon discussed above, wherein the region of the (M_2, M_3)-plane for which $x_{\rm peak} > x_{\rm thresh}$ decreases over time. However, after stasis begins, this region begins to grow again. As a result, the logarithmic slopes $\partial\Gamma_+(M,t)/\partial\log t$ and $\partial\Gamma_-(M,t)/\partial\log t$ both begin to increase. Indeed, for larger values of M, this effect persists for a sufficiently long duration that $\Gamma_+(M)$ and $\Gamma_-(M)$ both experience a temporary phase of growth. However, $\Gamma_+(M)$ and $\Gamma_-(M)$ begin to decrease again once the effect of evaporation — as reflected in the ever-increasing value of $M_{\rm cut}$ — begins to impact regions of the (M_2, M_3)-plane which otherwise would have contributed significantly to $\Gamma_+(M)$ and $\Gamma_-(M)$.

Interestingly, we also observe that there is an additional effect which becomes relevant for values of α near the maximum of its allowed range. Indeed, within the bottom two panels of Fig. 4 — and particularly in the bottom right panel — we observe that $\partial\Gamma_+(M,t)/\partial\log t$ and $\partial\Gamma_-(M,t)/\partial\log t$ initially *decrease* during the stasis epoch, prior to experiencing the increase which results from the effect described above. As a result, a pronounced "dip" appears in the $\Gamma_+(M)$ and $\Gamma_-(M)$ curves for $M = M_{\rm max}$.

We can understand the emergence of this dip by considering how $x_{\rm peak}$, $x_{\rm thresh}$, and x_p behave in the formal $\alpha \to -1$ limit. After some algebra, one finds that in this limit the expressions in Eqs. (5.22) and (3.15) reduce to

$$\begin{aligned} x_{\rm peak} &\to \widetilde{x}\left(\frac{2a_s}{a_{\rm MRE}}\right)^{1/3} \\ x_{\rm thresh} &\to \widetilde{x}\left(\frac{2a_s}{a_{\rm MRE}}\right)^{1/3} \\ x_p &\to \widetilde{x}\left(\frac{2a_s}{a_{\rm MRE}}\right)^{1/3}\left(\frac{\max\{M_1, M_2\}}{M_1+M_2}\right)^{1/3} . \end{aligned} \tag{5.24}$$

In other words, $x_{\rm peak}$ and $x_{\rm thresh}$ coincide in this limit, while x_p only differs from these other two quantities by

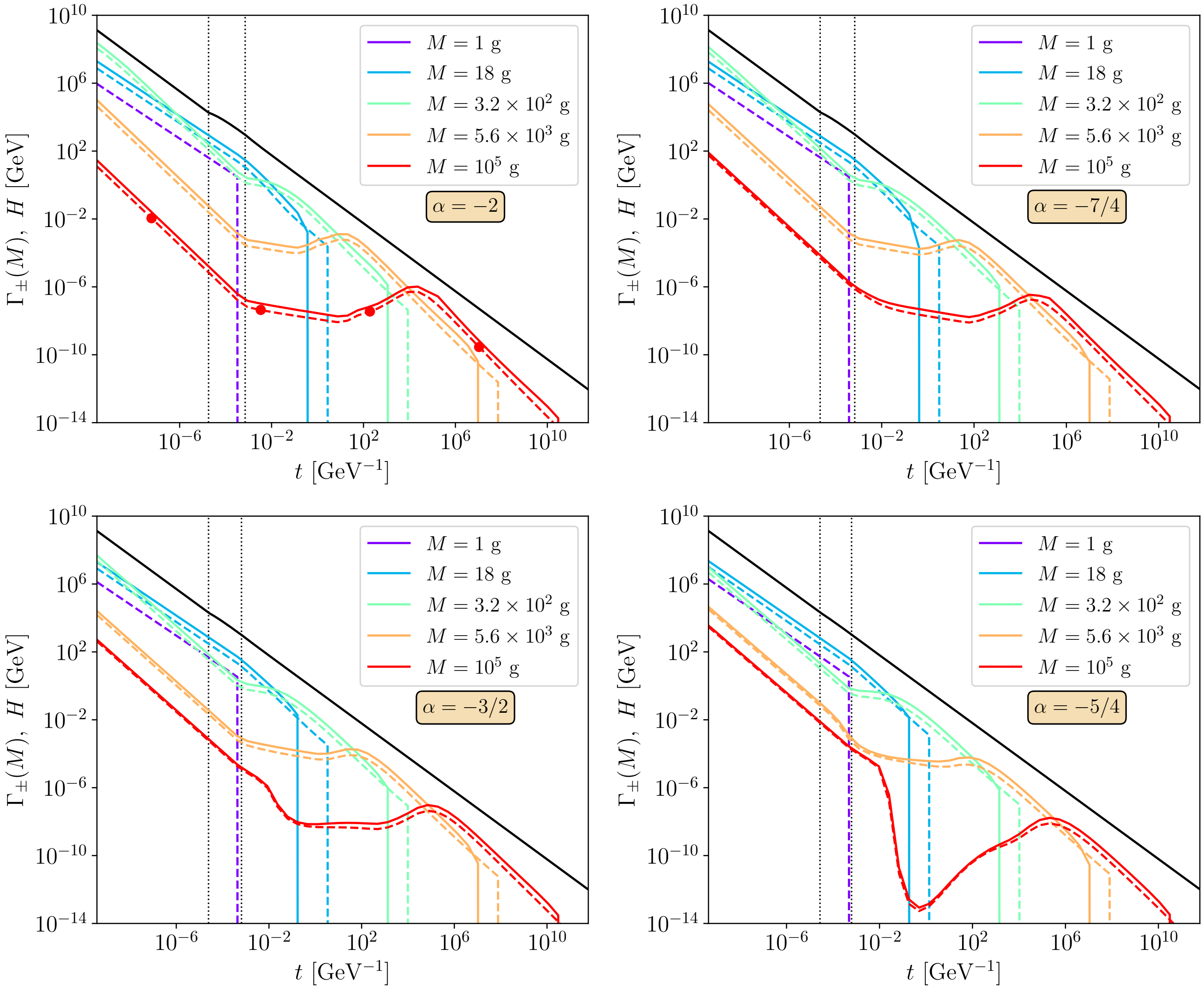

Fig. 4. The merger rates $\Gamma_+(M)$ (solid colored curves) and $\Gamma_-(M)$ (corresponding dashed curves), as well as the expansion rate H, shown as functions of time within the range $t_i < t < t_s$ for a variety of different values of M. The different panels of the figure correspond to different choices of α, and the results shown in all panels correspond to the parameter choices $M_{\rm min} = 1$ g, $M_{\rm max} = 10^5$ g, and $\mathcal{N}_{\rm PBH} = 2$. The four red dots indicated along the $M = 10^5$ g curve in the upper left panel correspond to the four t values for which $\Gamma_3(M_1, M_2, M_3)/H_{\rm PBH}$ is plotted for this M_1 value in Fig. 3. Since it is always the case that $\Gamma_+(M_{\rm min}) = 0$, only a dashed curve appears in any of the four panels for $M = 1$ g.

a numerical factor that ranges between $2^{-1/3} \approx 0.794$ and 1, depending on the relationship between M_1 and M_2. We also note that all three of these quantities are independent of M_3 in this limit.

As we move away from the strict $\alpha \to -1$ limit and consider values of α which are close to but not precisely equal to -1, we find that $x_{\rm peak}$, $x_{\rm thresh}$, and x_p remain quite similar. However, $x_{\rm peak}$ and $x_{\rm thresh}$ are in general no longer precisely equal and do depend — though not terribly sensitively — on M_3. Moreover, for such values of α, the range of x within which $\mathcal{I}(x)$ is non-negligible reduces to a narrow spike around $x \approx x_{\rm peak}$. Thus, if we consider how $\Gamma_3(M_1, M_2, M_3)$ depends on M_3 for fixed M_1 and M_2 at any time $t < t_{\rm PBH}$, we find that this differential merger rate is negligible for small M_3 and increases abruptly once M_3 reaches the critical value at which $x_{\rm thresh}$ drops below $x_{\rm peak}$ and this spike enters the integration region. However, since x_p is also very close to $x_{\rm peak}$, only a small additional increase in M_3 beyond this critical value results in the spike falling below x_p and $\Gamma_3(M_1, M_2, M_3)$ once again becoming negligible. Thus, for α within this regime, the value of $\Gamma_3(M_1, M_2, M_3)$ is non-negligible only within a narrow band within the (M_2, M_3)-plane.

The location of this band within the (M_2, M_3)-plane depends on the value of M_1. In particular, Eq. (5.16) implies that for larger M_1, the band is located at smaller values of M_2 and larger values of M_3. Moreover, regardless of the value of M_1, at times $t < t_{\rm PBH}$, the band shifts as t increases toward smaller values of M_2 and larger values of M_3. Thus, for large $M_1 \sim M_{\rm max}$, it migrates over time into the corner of the (M_2, M_3)-plane where $M_2 \sim M_{\rm min}$ and $M_3 \sim M_{\rm max}$ — the region of the plane wherein the coalescence time τ_m is maximized. While this migration is a universal behavior which occurs for all α, the region of the (M_2, M_3)-plane within which $\Gamma_3(M_1, M_2, M_3)$ is non-negligible is significantly broader for lower values of α.

Once stasis begins, however, the PBHs with $M \sim M_{\rm min}$ rapidly evaporate, and the binary configurations for which $\Gamma_3(M_1, M_2, M_3)$ is sizable vanish long before they have the opportunity to coalesce. As a result $\Gamma_+(M, t)$ and $\Gamma_-(M, t)$ drop precipitously. Eventually, as t further increases and the region of the (M_2, M_3)-plane within which $\Gamma_3(M_1, M_2, M_3)$ is sizable broadens, these rates begin to grow again and eventually become comparable to the corresponding rates obtained for smaller values of α.

By far the most important message of Fig. 4, however, is that in all four panels of the figure, $\Gamma_+(M)$ and $\Gamma_-(M)$ both remain well below H for all $M_{\rm min} < M < M_{\rm max}$ throughout the entire period from $t_i < t < t_s$. The effect of mergers on $f_{\rm BH}(M, t)$ is therefore negligible in comparison with the effect of expansion throughout this period. We therefore conclude that the shape of $f_{\rm BH}(M, t)$ is not significantly distorted by mergers either prior to or during the stasis epoch. In other words, we conclude that $M_D = M_{\rm max}$. Moreover, while the results shown in Fig. 4 reflect the particular choices of $M_{\rm min}$, $M_{\rm max}$, and $\mathcal{N}_{\rm PBH}$ that we have adopted for purposes of illustration therein, we have verified that the same conclusions hold for essentially any other viable combination of these model parameters as well. Thus, we conclude that mergers between PBHs have only a negligible impact on the dynamics which give rise to stasis in our PBH-induced stasis model and can therefore be ignored.

VI. ACCRETION

In general, the contribution $(dM/dt)_{\rm acc}$ to the rate at which the mass M of a given PBH changes as a result of accretion within the early universe depends on M itself, on the cosmological expansion rate, and on the nature of the material being accreted. The effect of accretion on PBH masses has been investigated extensively within the context of the thermal expansion history associated with the standard cosmology [47–52]. In this section, we examine its effect within the context of our PBH-induced stasis cosmology.

Within the regime in which the Schwarzschild radius of the PBH is much smaller than the Hubble horizon, $(dM/dt)_{\rm acc}$ may be estimated by means of a quasi-stationary approximation [53, 54]. In this approximation, the effect of cosmological expansion is neglected except for its impact on the energy density of the universe, which is still taken to be approximately equal to $\rho_{\rm crit}$ at large distances away from the PBH. Applying this quasi-stationary approximation to the case of an isolated Schwarzschild black hole of mass M immersed in a perfect fluid with cosmological abundance Ω_F and equation-of-state parameter $0 < w_F < 1$, one may derive an expression for $(dM/dt)_{\rm acc}$, which takes the form [55, 56]

$$\left(\frac{dM}{dt}\right)_{\rm acc} = \frac{4\pi A(w_F) M^2 (1 + w_F)\Omega_F \rho_{\rm crit}}{M_P^4} , \qquad (6.1)$$

where $A(w_F)$ is a numerical factor which depends on w_F. Formally, for a fluid with a constant value of $0 < w_F < 1$, one finds that this numerical factor is given by [56]

$$A(w_F) = \frac{(1 + 3w_F)^{(1+3w_F)/(2w_F)}}{4w_F^{3/2}} , \qquad (6.2)$$

which has the property that $A(w_F) > 4$ for all w_F within this range. However, this expression diverges in the $w_F \to 0$ limit and is valid only within the regime in which w_F differs significantly from zero.

The effect of accretion in the opposite regime has been examined by a number of authors [57–59] — typically in the context in which the fluid with $w_F \approx 0$ is a gas of non-relativistic particles which represents a significant fraction of the total energy density of the universe. The results of these studies suggest that the effect of accretion on PBH masses can indeed be substantial in this regime, though there exist significant uncertainties as to its quantitative impact. Thus, while it is likely that the accretion of a fluid with $w_F \approx 0$ and $\Omega_F \sim \mathcal{O}(1)$ onto a population of PBHs for a protracted period would induce distortions in the shape of $f_{\rm BH}(M, t)$, the precise extent to which this effect constrains the emergence or duration of stasis within the parameter space of our model is unclear.

Within the context of this model, the only fluid with a non-negligible abundance which can accrete onto the PBHs and which can potentially have an equation-of-state parameter near zero is the perfect fluid which dominates the energy density of the universe during the PBH-formation epoch, which has $w_c \approx 0$ when α is near the maximum of its allowed range. In what follows, we shall therefore focus primarily on the regime wherein α is not too close to this maximum value and $(dM/dt)_{\rm acc}$ can reliably be modeled using the expression in Eq. (6.1). More specifically, we focus on the regime in which $\alpha < -1.2$, for which $w_c > 1/9$.

During the PBH-formation epoch, the material accreted by the PBHs is the perfect fluid which dominates the energy density of the universe. Thus, during this epoch, $\Omega_F = 1$ and $w_F = w_c$. However, since the Schwarzschild radius of a PBH is comparable to the size of the Hubble horizon at the time it forms due to gravitational collapse, cosmological expansion has a significant effect on the accretion rate [60, 61]. The quasi-stationary approximation on which Eq. (6.1) is predicated is therefore unreliable for a PBH of initial mass M_i

until $H^{-1} \gg 2GM_i$ — or, equivalently, until $t \gg t_p(M_i)$. In what follows, for concreteness, we shall assume that this approximation can safely be invoked for such a PBH at times $t > \theta_{\rm QS} t_p(M_i)$, where $\theta_{\rm QS} \gg 1$ is independent of M_i.

There exists some uncertainty regarding the manner in which a PBH of initial mass M_i evolves from $t_p(M_i)$ until the time at which the quasi-stationary approximation becomes valid. Nevertheless, it has been shown [60, 62–65] that the sustained period of rapid, self-similar growth which would appear to follow from Eq. (6.1) for a PBH with a radius comparable to the Hubble horizon does not in fact occur — at least in situations in which w_F differs significantly from zero. Moreover, for such values of w_F, it is commonly assumed that $(dM/dt)_{\rm acc}$ is small and that its effect on M is not terribly significant [28]. In what follows, we shall therefore assume that the mass of a PBH is not significantly modified from M_i while the Hubble horizon remains comparable to its Schwarzschild radius. We shall consider the implications of relaxing this assumption in Sect. VII.

By contrast, once $t \gg t_p(M_i)$ and $(dM/dt)_{\rm acc}$ can reliably be approximated using Eq. (6.1), evaluating the effect of accretion on the PBH mass spectrum is far more straightforward. Indeed, this equation implies that

$$\frac{dM}{dt} ~=~ \left[\frac{2A_F(w_c)}{3(1+w_c)M_P^2}\right]\frac{M^2}{t^2} \tag{6.3}$$

during the remainder of the PBH-formation epoch. Solving this equation, we find that the mass of a PBH during the stasis epoch is given at times $t_p(M_i) \ll t < t_f$ by

$$M(t) ~=~ M_i\left[1 - C_f(w_c)\left(1 - \frac{\theta_{\rm QS} t_p(M_i)}{t}\right)\right]^{-1} ~, \tag{6.4}$$

where we have defined

$$C_f(w_c) ~\equiv~ \frac{2A_F(w_c)M_i}{3M_P^2(1+w_c)\theta_{\rm QS} t_p(M_i)} ~=~ \frac{\gamma A_F(w_c)}{2\theta_{\rm QS}} ~. \tag{6.5}$$

Since $C_f(w_c)$ is independent of M_i, it follows that within the regime in which $t_f \gg \theta_{\rm QS} t_i$ — the regime in which the quasi-static approximation becomes valid for our entire population of PBHs well before the PBH-formation epoch ends — the mass of every PBH at $t = t_f$ is rescaled relative to its corresponding initial mass by an effectively universal factor. In particular, taking $\gamma = 1$, we have

$$M(M_i, t_f) ~\approx~ M_i\left[1 - \frac{A_F(w_c)}{2\theta_{\rm QS}}\right]^{-1} ~. \tag{6.6}$$

Within this regime, then, the PBH mass spectrum at $t = t_f$ is

$$f_{\rm BH}(M, t_f) ~=~ \left(\frac{a}{a_i}\right)^{-3}\left[1 - \frac{A_F(w_c)}{2\theta_{\rm QS}}\right]^{1-\alpha} f_{\rm BH}(M_i, t_i) ~. \tag{6.7}$$

In other words, the overall normalization of $f_{\rm BH}(M,t)$ is increased relative to what it otherwise would have been in the absence of accretion, and the range of masses within the spectrum is shifted upward, but the overall power-law scaling behavior of $f_{\rm BH}(M,t)$ with M — and even the value of the power-law exponent — remains unchanged. Moreover, for $\alpha < -1.2$, we find that the proportional increase in the the mass of each PBH during the period from $t_p(M_i)$ to t_f is bounded from above by $[M(M_i,t_f) - M_i]/M_i \lesssim 0.33$. Thus, we conclude that the effect of accretion on the range of PBH masses during the PBH-formation epoch is not terribly significant for values of α within this regime.

Given that the effect of accretion on $f_{\rm BH}(M,t)$ within this regime is simply an overall rescaling accompanied by a shift in the range of M for which this function receives non-vanishing support, we note that this effect can be compensated by a redefinition of $M_{\rm min}$, $M_{\rm max}$, and $\mathcal{N}_{\rm PBH}$. In other words, the apparent values of these parameters at $t = t_f$ are different — and all slightly larger — than they would have been in the absence of accretion. However, since these shifts are indeed quite slight, their impact on the results of the merger-rate analysis we performed in Sect. V, as well as on other aspects of our PBH-induced stasis cosmology, is insignificant. Throughout the remainder of this section, we shall account for the effect of accretion within the regime in which $t_f \gg \theta_{\rm QS} t_i$ via such a redefinition of $M_{\rm min}$, $M_{\rm max}$, and $\mathcal{N}_{\rm PBH}$. In other words, we shall redefine M_i such that $M_i \rightarrow M(M_i, t_f)$.

By contrast, within the regime in which $t_f \sim \theta_{\rm QS} t_i$, the factor by which M increases relative to M_i between $t_p(M_i)$ and t_f is not independent of M_i. Within this regime, distortions to $f_{\rm BH}(M,t)$ can arise and the effect of accretion cannot be accounted for via a redefinition of $M_{\rm min}$, $M_{\rm max}$, and $\mathcal{N}_{\rm PBH}$. Thus, such distortions *can* meaningfully impact the dynamics which give rise to stasis.

Nevertheless, there are reasons why the impact of these distortions on the expansion history is not expected to be particularly severe. First of all, they arise only at the upper end of the PBH mass spectrum. Indeed, since the collapse time scales with M_i as $t_p(M_i) \sim M_i$, the distortions in the shape of $f_{\rm BH}(M_i, t_f)$ which arise due to accretion are only meaningful for $M_i \sim M_{\rm max}$. By contrast, for PBHs with $M_i \ll M_{\rm max}$ the collapse time is such that $t_f \gg \theta_{\rm QS} t_p(M_i)$. The factor by which M increases relative to M_i for these lighter PBHs is therefore effectively independent of M_i and given by Eq. (6.6). This implies that distortions to the PBH mass spectrum which develop during the PBH-formation epoch do not disrupt stasis outright, but at worst result in the stasis epoch ending prematurely by a few e-folds, at the point when the evaporation of the heavier PBHs would have become important for sustaining stasis. Moreover, as discussed above, even when distortions to $f_{\rm BH}(M,t)$ do arise, the magnitude of the distortions is at most at the 33% level. Thus, the impact of these distortions on the matter abundance $\Omega_{\rm BH}$ as the system begins to depart from stasis is far from dramatic.

One criterion which can be used to quantify the extent of these distortions is the ratio of the factor $M(M_{\rm min}, t_f)/M_{\rm min}$ by which the mass of a PBH with $M_i = M_{\rm min}$ grows during the PBH-formation epoch to the factor $M(M_{\rm max}, t_f)/M_{\rm max}$ by which the mass of a PBH with $M_i = M_{\rm max}$ grows during this epoch. In particular, the impact of these distortions on stasis should be negligible whenever the criterion $J \ll 1$ is satisfied, where we have defined

$$J \;\equiv\; \frac{M(M_{\rm min}, t_f)M_{\rm max}}{M(M_{\rm max}, t_f)M_{\rm min}} - 1 \;. \tag{6.8}$$

By contrast, when this criterion is not satisfied, the stasis epoch ends prematurely, as discussed above, but still can be of significant duration.

As the universe enters the PBH-dominated epoch, the contribution to energy density of the universe from the perfect fluid which dominated that energy density during the PBH-formation epoch becomes subleading. Nevertheless, PBHs can still accrete material from this fluid during the PBH-dominated epoch. Thus, once again, we have $w_F = w_c$. However, the abundance $\Omega_F(t)$ during the PBH-dominated epoch evolves with time according to the relation

$$\Omega_F(t) \;\approx\; \frac{1}{2}\left(\frac{t}{t_f}\right)^{-2w_c} \;, \tag{6.9}$$

where we have taken $\Omega_F(t_f) = 1/2$ at the transition point between the two epochs. As a result, Eq. (6.1) reduces to

$$\left(\frac{dM}{dt}\right)_{\rm acc} \;=\; \left[\frac{(1+w_c)A(w_c)t_f^{2w_c}}{3M_P^2}\right]\frac{M^2}{t^{2(1+w_c)}} \;. \tag{6.10}$$

during this epoch. Solving this differential equation for M, we find that

$$M(t) \;=\; M(t_f)\left[1 - C_{\rm PBH}(w_c)\left(1 - \frac{t_f^{1+2w_c}}{t^{1+2w_c}}\right)\right]^{-1} \;, \tag{6.11}$$

where we have defined

$$C_{\rm PBH}(w_c) \;\equiv\; \frac{(1+w_c)A(w_c)M(t_f)}{3(1+2w_c)M_P^2\, t_f} \;. \tag{6.12}$$

We note that $C_{\rm PBH}(w_c)$, unlike $C_f(w_c)$, depends nontrivially on M_i. As a result, accretion during this epoch leads to distortions in the shape of $f_{\rm BH}(M, t)$ across the entire PBH mass spectrum.

Since we compensate for the effect of accretion during the PBH-formation epoch via a redefinition of M_i, as discussed above, we take $M(t_f) = M_i$ in Eqs. (6.11) and (6.12). We also note that in deriving Eq. (6.11), we have assumed that the quasi-stationary approximation is valid at all times $t_f < t < t_{\rm PBH}$, and thus that $2M_{\rm max}GH(t_f) \ll 1$.

Finally, during the stasis epoch, the surrounding fluid is the radiation into which the PBHs decay, so we have $\Omega_F = \overline{\Omega}_\gamma$ and $w_F = 1/3$. Since the value of $w = \overline{w}$ for the universe as a whole is also effectively constant during this epoch, we have

$$\rho_{\rm crit} \;=\; \frac{M_P^2}{6\pi(1+\overline{w})^2 t^2} \;. \tag{6.13}$$

As discussed below Eq. (2.4), most of the mass lost by a PBH of mass M as it evaporates is lost at times $t \sim \tau_e(M)$. Thus to a good approximation, we may ignore the effect of evaporation on the evolution of M at times $t \ll \tau_e(M)$. Thus, during the stasis epoch, $(dM/dt)_{\rm acc}$ represents the only potentially non-negligible contribution to the overall rate of change of M. Since the quasi-stationary approximation on which Eq. (6.1) is predicated is indeed valid during this epoch, we have

$$\frac{dM}{dt} \;=\; \left[\frac{16\sqrt{3}\,\overline{w}}{(1+\overline{w})^2 M_P^2}\right]\frac{M^2}{t^2} \;. \tag{6.14}$$

Solving this equation, we find that the mass of a PBH during the stasis epoch is given at times $t_{\rm PBH} \lesssim t \ll \tau_p(M)$ by

$$M(t) \;=\; M(t_{\rm PBH})\left[1 - C_s(\overline{w})\left(1 - \frac{t_{\rm PBH}}{t}\right)\right]^{-1} \;, \tag{6.15}$$

where the mass $M(t_{\rm PBH})$ of the PBH at the beginning of the stasis epoch is given by taking $t = t_{\rm PBH}$ in Eq. (6.11) and where we have defined

$$C_s(\overline{w}) \;\equiv\; \frac{16\sqrt{3}\,\overline{w}M(t_{\rm PBH})}{(1+\overline{w})^2 M_P^2 t_{\rm PBH}} \;. \tag{6.16}$$

In order to assess the net effect of accretion on the mass of an individual PBH during the PBH-domination and stasis epochs, we consider the proportional increase in mass

$$\frac{\Delta M}{M} \;\equiv\; \frac{M(M_i, \tau_e(M_i)) - M_i}{M_i} \tag{6.17}$$

that such a PBH experiences during the period from t_f until the time $\tau_e(M_i)$ at which it would have completely evaporated in the absence of accretion.

Since the evaporation time of a PBH increases with M in accord with Eq. (2.4), a PBH which would have evaporated at $t = \tau_e(M_i)$ in the absence of accretion would still exist at this time if it accretes material at any time after it was produced. Moreover, Eqs. (6.11) and (6.11) indicate that $\Delta M/M$ increases with M across any particular population of PBHs. This implies that if the value $(\Delta M/M)_{\rm max}$ obtained by taking $M_i = M_{\rm max}$ within such a population is negligible, the effect of accretion is negligible across the entire PBH mass spectrum. Given this, we focus on evaluating $(\Delta M/M)_{\rm max}$ in what follows.

In order to determine in which regions of the parameter space of our PBH-induced stasis model the criterion $(\Delta M/M)_{\rm max} \ll 1$ is satisfied, we survey that parameter space numerically, using the full expressions in Eqs. (6.11) and (6.15). However, we also note that a reasonably simple analytic approximation for this condition can be formulated in a straightforward manner. Indeed, within the regime in which $\Delta M/M \ll 1$, the second term within the square brackets in each of Eqs. (6.11) and (6.15) is much less than unity. Expanding $\Delta M/M$ and retaining terms up to linear order in each of these small dimensionless quantities and taking $M_i = M_{\rm max}$ yields

$$\left(\frac{\Delta M}{M}\right)_{\rm max} \approx M_{\rm max}\Bigg\{C_{\rm PBH}(w_c)\left[1-\left(\frac{t_f}{t_{\rm PBH}}\right)^{1+2w_c}\right] + C_s(\overline{w})\left(1-\frac{t_{\rm PBH}}{\tau_e(M_i)}\right)\Bigg\} \tag{6.18}$$

at $t = \tau_e(M_{\rm max})$. Making use of Eqs. (6.12) and (6.16), along with the fact that

$$\frac{t_{\rm PBH}}{t_f} = \left(\frac{a_f}{a_{\rm PBH}}\right)^{3/2} = e^{-3\mathcal{N}_{\rm PBH}/2} , \tag{6.19}$$

in order to simplify this result, we find that the condition under which $\Delta M/M \ll 1$ for all $M_{\rm min} \leq M \leq M_{\rm max}$ can be expressed as

$$\frac{M_{\rm min}^3}{M_{\rm max}} \gg \epsilon M_P^2\left[\frac{48\sqrt{3}\overline{w}}{(1+\overline{w})^2}\left(1-\frac{M_{\rm min}^3}{M_{\rm max}^3}\right) + \frac{(1+w_c)A(w_c)}{1+2w_c}\left(e^{3\mathcal{N}_{\rm PBH}/2} - e^{-3w_c\mathcal{N}_{\rm PBH}}\right)\right] . \tag{6.20}$$

Within the regime in which $M_{\rm min} \ll M_{\rm max}$ and $\mathcal{N}_{\rm PBH} \gtrsim 1$, this relation reduces to

$$\frac{M_{\rm min}^3}{M_{\rm max}} \gg \left[\frac{48\sqrt{3}\overline{w}}{(1+\overline{w})^2} + \frac{(1+w_c)A(w_c)}{1+2w_c}e^{3\mathcal{N}_{\rm PBH}/2}\right]\epsilon M_P^2 . \tag{6.21}$$

Indeed, since $M_{\rm min} \ll M_{\rm max}$ within our region of interest for stasis in this scenario, this more compact formulation of the $(\Delta M/M)_{\rm mmax} \ll 1$ condition is valid throughout the vast majority of our parameter-space region of interest. Qualitatively, it is clear from Eq. (6.21) that the regions of parameter space within which the effect of accretion on $f(M,t)$ is the most significant are those in which $M_{\rm min}$ is near its lower limit, $M_{\rm max}$ is near its upper limit, and $\mathcal{N}_{\rm PBH}$ is large. It is also apparent from Eq. (6.21) that the corresponding constraint contour is not particularly sensitive to the value of α, except within the regime in which α is very close to -1 and $A(w_c)$ is therefore extremely large. However, as we have discussed above, the expression for $A(w_c)$ in Eq. (6.2) is likely unreliable in this regime, and in what follows, we restrict our consideration to values of α within the range $-2 < \alpha < -1.2$.

We now present the results of our numerical analysis. In Fig. 5, we show contours of $(\Delta M/M)_{\rm max}$ within the $(\alpha, M_{\rm min})$-plane at the time $t = \tau_e(M_{\rm max})$. The left panel shows the results for $M_{\rm max} = 10^7$ g and $\mathcal{N}_{\rm PBH} = 2$, the middle panel shows the results for $M_{\rm max} = 10^7$ g and $\mathcal{N}_{\rm PBH} = 8$, and the right panel shows the results for $M_{\rm max} = 10^9$ g and $\mathcal{N}_{\rm PBH} = 2$. Within the gray region at the bottom of each figure, $(\Delta M/M)_{\rm max} > 0.01$, indicating a non-negligible change in M for at least the heaviest PBHs. The red hatched region in each panel indicates the portion of the plane within which PBHs with $M_i = M_{\rm max}$ form sufficiently close to the end of the PBH-formation epoch that their Schwarzschild radii are still comparable in size to the Hubble horizon and the quasi-stationary approximation underlying Eq. (6.1) is therefore unreliable. More precisely speaking, this region corresponds to the portion of the plane wherein $2MGH(t_f) > 0.01$. The yellow hatched region in the middle panel indicates the region wherein the consistency condition $\mathcal{N}_{\rm PBH} < \mathcal{N}_{\rm PBH}^{(\rm max)}$ is violated. However, we note that since this constraint represents that requirement that PBHs with $M_i = M_{\rm max}$ are produced before t_f, it is in a sense simply a weaker version of the constraint indicated by the red hatched region. Throughout the region above the orange dashed contour in each panel, the condition $J < 0.01$ is satisfied for $\theta_{\rm QS} = 100$. Below this contour, distortions develop near the upper end of the mass spectrum during the PBH-formation epoch and stasis concludes a few e-folds earlier than it otherwise would have.

We observe that there exists a significant region of parameter space within each panel of Fig. 5 wherein $(\Delta M/M)_{\rm max} < 0.01$ and $J < 0.01$, while the other consistency conditions we have imposed are likewise satisfied. The effect of accretion on the spectrum of PBHs throughout this entire region is negligible. We also observe that $(\Delta M/M)_{\rm max}$ decreases substantially as $M_{\rm min}$ increases, but that this quantity is not terribly sensitive to the value of α — provided of course that α is not too close to -1 and the expression in Eq. (6.1) therefore remains valid. Comparing the results across the three panels of the figure, we also observe that our negligibility condition $(\Delta M/M)_{\rm max} < 0.01$ becomes more constraining within the (α, M_1)-plane as either $M_{\rm max}$ or $\mathcal{N}_{\rm PBH}$ increases.

Taken together, the results shown in Fig. 5 indicate that unless $\mathcal{N}_{\rm PBH}$ is quite large, $M_{\rm min}$ is near the minimum of its allowed range, and $M_{\rm max}$ is near the maximum of its allowed range, the net effect of accretion on the masses of all PBHs within the mass spectrum of our PBH-induced stasis model — and therefore on the shape of $f_{\rm BH}(M,t)$ — can safely be ignored. Indeed, we note that all of the results presented in Figs. 5 and 6 of Ref. [15] correspond to combinations of model parameters for which the negligibility condition $(\Delta M/M)_{\rm max} < 0.01$ is satisfied.

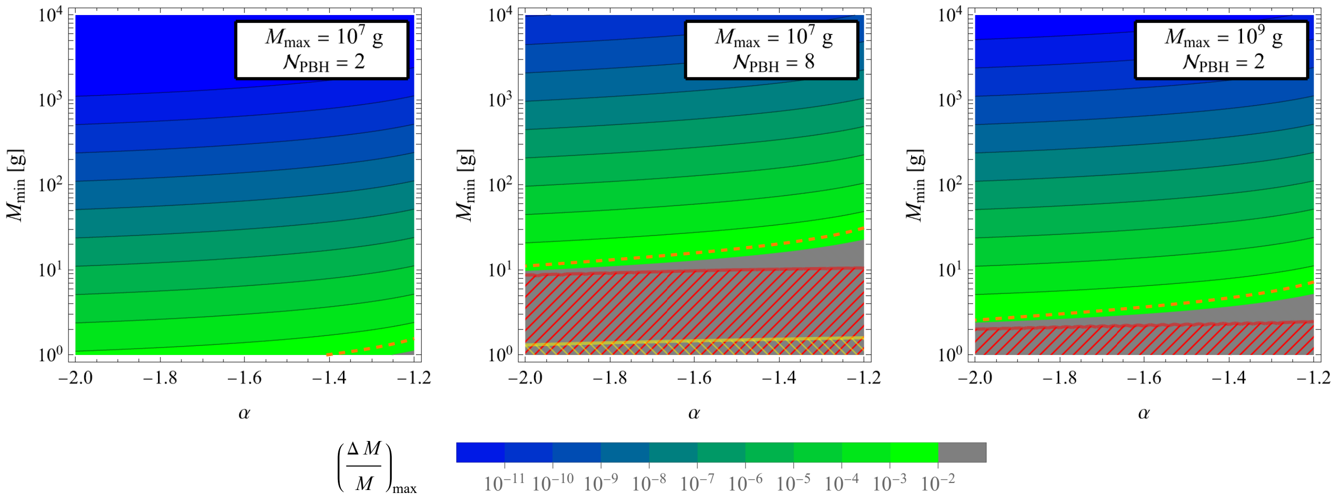

Fig. 5. Contours of $(\Delta M/M)_{\rm max}$ within the $(\alpha, M_{\rm min})$-plane at the time $t = \tau_e(M_{\rm max})$ at which a PBH with $M_i = M_{\rm max}$ would have evaporated completely in our stasis cosmology in the absence of accretion — *i.e.*, at the time at which the stasis epoch would have ended. The left panel shows the results for $M_{\rm max} = 10^7$ g and $\mathcal{N}_{\rm PBH} = 2$, the middle panel shows the results for $M_{\rm max} = 10^7$ g and $\mathcal{N}_{\rm PBH} = 8$, and the right panel shows the results for $M_{\rm max} = 10^9$ g and $\mathcal{N}_{\rm PBH} = 2$. Within the gray region at the bottom of each panel, $(\Delta M/M)_{\rm max} > 0.01$, indicating a non-negligible change in M for at least the heaviest PBHs. The red hatched region in each panel indicates the region within which PBHs with $M_i = M_{\rm max}$ form sufficiently close to the end of the PBH-formation epoch that the quasi-stationary approximation underlying Eq. (6.1) may not be reliable. The yellow hatched region at the bottom of the middle panel indicates the region of the $(\alpha, M_{\rm min})$-plane within which the consistency condition $\mathcal{N}_{\rm PBH} < \mathcal{N}_{\rm PBH}^{(\rm max)}$ is violated. Throughout the region above the orange dashed contour in each panel, the condition $J < 0.01$ is satisfied for $\theta_{\rm QS} = 100$.

We have shown that the effect of accretion on the masses of the individual PBHs within our mass spectrum is negligible throughout a significant portion of our parameter-space region of interest. However, while $(\Delta M/M)_{\rm max} \ll 1$ is certainly a necessary condition for ensuring that the dynamics which give rise to stasis is not disturbed by accretion, it is not a sufficient one. We must also verify that the total rate $\Gamma_{\rm ac}$ at which energy density is transferred from radiation to matter by accretion across the entire cosmological population of PBHs is sufficiently small throughout the stasis epoch that it can be neglected. Indeed, while the rate Γ_e at which energy density is transferred due to evaporation is dominated at an any particular time during this epoch by PBHs with masses M only slightly above $\widetilde{M}(t)$, the fact that $(dM/dt)_{\rm ac} \sim M^2$ implies that PBHs with a far broader range of M contribute non-negligibly to $\Gamma_{\rm ac}$. In general, then, we must require that $\Gamma_{\rm ac} \ll \Gamma_e$ throughout this epoch.

In general, the energy-transfer rate due to accretion may be expressed as

$$\Gamma_{\rm ac} \;=\; \frac{1}{\rho_{\rm BH}} \int_0^\infty dM\, f_{\rm BH}(M,t) \left(\frac{dM}{dt}\right)_{\rm ac} . \tag{6.22}$$

Since our goal is simply to determine the region of our model parameter space wherein the condition $\Gamma_{\rm ac} \ll \Gamma_e$ is violated, we proceed by evaluating $\Gamma_{\rm ac}$ for the simple form of $f_{\rm BH}(M,t)$ in Eq. (5.1). During the stasis epoch, $(dM/dt)_{\rm ac}$ is given by Eq. (6.14), while

$$\frac{a_i^3 \rho_{{\rm BH},i}}{a^3 \rho_{\rm BH}} \;=\; \frac{\rho_{\rm crit}(t_{\rm PBH}) r^3(t_{\rm PBH})}{\rho_{\rm crit}(t) r^3(t)} \;=\; \left(\frac{t}{t_{\rm PBH}}\right)^{2\overline{w}/(1+\overline{w})} . \tag{6.23}$$

We therefore have

$$\Gamma_{\rm ac} \;=\; \frac{16\sqrt{3}\,\overline{w}(\alpha+1)}{(1+\overline{w})^2 M_P^2 t^2 (M_{\rm max}^{\alpha+1} - M_{\rm min}^{\alpha+1})} \times \left(\frac{t}{t_{\rm PBH}}\right)^{2\overline{w}/(1+\overline{w})} \int_{\widetilde{M}(t)}^{M_{\rm max}} dM_i M_i^{\alpha+1} . \tag{6.24}$$

By contrast, the energy-transfer rate due to evaporation was shown in Ref. [15] to be $\Gamma_e = -(\alpha+1)/(3t)$. Thus, through use of Eq. (2.9), we obtain an expression for the ratio $\Gamma_{\rm ac}/\Gamma_e$ of the form

$$\frac{\Gamma_{\rm ac}}{\Gamma_e} \;=\; \frac{144\sqrt{3}\,\overline{w}\epsilon}{(1+\overline{w})^2} \left(\frac{t}{t_{\rm PBH}}\right)^{(\overline{w}-1)/(\overline{w}+1)} \left(\frac{M_P}{M_{\rm min}}\right)^2 \times \begin{cases} \dfrac{1}{\alpha+2}\left[\dfrac{M_{\rm max}^{\alpha+2} - \widetilde{M}^{\alpha+2}(t)}{M_{\rm min}(M_{\rm min}^{\alpha+1} - M_{\rm max}^{\alpha+1})}\right] & -2 < \alpha < -1 \\ \left(1 - \dfrac{M_{\rm min}}{M_{\rm max}}\right)^{-1} \log\left(\dfrac{M_{\rm max}}{\widetilde{M}(t)}\right) & \alpha = -2 \, . \end{cases} \tag{6.25}$$

We note that for $0 < \overline{w} < 1/3$ this ratio decreases monotonically with t. This is primarily due to the fact that the accretion rate is proportional to the energy density of the background radiation, which scales like $\rho_\gamma \sim t^{-2}$ during stasis, whereas $\Gamma_e \sim t^{-1}$ must scale in the same manner with t as does H in order for stasis to be maintained. It will therefore be sufficient for us to require that $\Gamma_{\rm ac} \ll \Gamma_e$ at the beginning of stasis, since if this condition is satisfied when $t = t_{\rm PBH}$ it will be satisfied for all $t_{\rm PBH} < t < t_s$ as well.

In Fig. 6, we display contours of $\Gamma_{\rm ac}(t_{\rm PBH})/\Gamma_e(t_{\rm PBH})$ within the $(\alpha, M_{\rm min})$-plane for $M_{\rm max} = 10^9$ g. (We need not specify $\mathcal{N}_{\rm PBH}$, as this ratio is independent of $\mathcal{N}_{\rm PBH}$). This choice of $M_{\rm max}$ yields the maximum possible value of $\Gamma_{\rm ac}(t_{\rm PBH})/\Gamma_e(t_{\rm PBH})$, given the constraint on $M_{\rm max}$ in Eq. (2.8). We observe that this ratio is much smaller than unity throughout the entire region of the $(\alpha, M_{\rm min})$-plane shown. Thus, we conclude that the net effect of accretion on the transfer of energy density between matter and radiation during stasis is always negligible in comparison with the net effect of evaporation.

In summary, given the results in Figs. 5 and 6, we conclude that the effect of accretion both on the masses of the individual PBHs and on the overall rate at which energy density is transferred between matter and radiation during the stasis epoch is negligible throughout the majority of our parameter-space region of interest. That said, we have also seen that accretion *does* impact the stasis dynamics within certain regions of that parameter space — in particular, those in which $\mathcal{N}_{\rm PBH}$ is large or in which the mass spectrum is particularly broad. Thus, we find that accretion yields meaningful constraints on the emergence of stasis within the context of PBH-induced stasis scenarios.

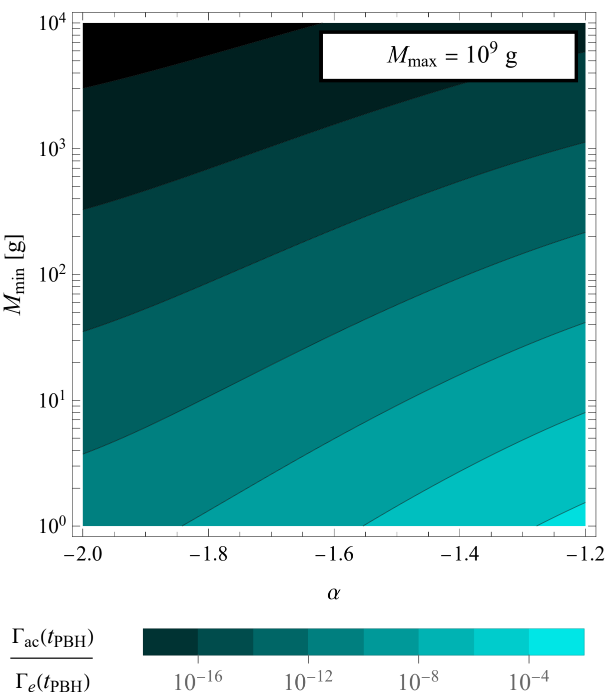

Fig. 6. Contours of $\Gamma_{\rm ac}(t_{\rm PBH})/\Gamma_e(t_{\rm PBH})$ within the $(\alpha, M_{\rm min})$-plane at the beginning of the stasis epoch, where $\Gamma_{\rm ac}$ denotes the total rate of energy-density transfer from radiation to PBHs from accretion and Γ_e denotes the total rate of energy-density transfer from PBHs to radiation from evaporation. The results shown correspond to the choice of $M_{\rm max} = 10^9$ g — a choice which yields the maximum value of this ratio subject to the constraint on $M_{\rm max}$ in Eq. (2.8).

VII. CONCLUSIONS

In this paper, we have examined how mergers and accretion affect the mass spectrum of PBHs in scenarios which give rise to cosmological stasis. While the effect of mergers is negligible for PBH masses within the relevant range, we find that accretion can have an effect on $f_{\rm BH}(M,t)$. However, this effect turns out to have a significant impact on $f_{\rm BH}(M,t)$ only in cases in which $\mathcal{N}_{\rm PBH}$ is large or in which $M_{\rm min}$ and $M_{\rm max}$ lie near the opposite endpoints of the phenomenologically allowed range of PBH masses specified in Eq. (2.8). By contrast, throughout the vast majority of the parameter-space region of interest for the PBH-induced stasis model we have examined here, the effect of accretion is negligible. This confirms that this model, the distinctive phenomenological signatures of which were discussed in Ref. [15], is indeed a viable realization of cosmological stasis.

Notably, these signatures include a number of effects on the gravitational-wave spectrum. Not only does the modification of the expansion history alter the profile of the primordial gravitational-wave background in a manner such that distortions to the present-day gravitational-wave background spectrum within different frequency ranges are correlated, but the enhancements to the primordial power spectrum which lead to the formation of the PBHs themselves also lead to an enhancement in the gravitational-wave background spectrum at higher frequencies. The observation of such a pattern of correlated gravitational-wave signatures would be compelling evidence that the universe indeed underwent an epoch of PBH-induced stasis. Moreover, any period of matter/radiation stasis leads to an enhanced growth of density perturbations on small scales [23], which can potentially lead to further observational signatures.

Several comments are in order. First, in this paper we have delineated the regions of the parameter space of our PBH-induced stasis model within which the stasis dynamics is not appreciably impacted by mergers and accretion. We have not, however, investigated what happens to $f_{\rm BH}(M,t)$ outside of these regions and what the resulting impact is on the expansion history. An analysis along these lines would reveal exactly to what extent the behavior of $\Omega_{\rm BH}$ and H deviates from stasis when these processes have a non-negligible impact on $f_{\rm BH}(M,t)$. We leave such a detailed study for future work.

Second, as discussed in Sect. VI, there exist significant uncertainties regarding the quantitative impact of accretion on the mass of a PBH during the period immediately following its production via gravitational collapse during the PBH-formation epoch. In this paper, we have assumed that the effect of accretion may either be neglected until the quasi-static approximation becomes valid or else may be absorbed via a redefinition of our model parameters. While arguments have been advanced in the literature which motivate these assumptions (for a review, see, *e.g.*, Ref. [61]), the fact that accretion can impact the dynamics which leads to stasis via its impact on the shape of $f_{\rm BH}(M,t)$ provides additional impetus for examining the effect that accretion has on a PBH during the period immediately following gravitational collapse.

Third, in this paper we have ignored the effect that binary formation has the accretion rate — a phenomenon which was examined in the context of the standard cosmology in Ref. [52]. Within highly asymmetric binaries, the accretion rate of the lighter PBH can be significantly enhanced by the increase in the density of the ambient fluid which results from the presence of the heavier PBH. These effects could in principle amplify the distortions which result from accretion, provided that a significant fraction of the lighter PBHs are in binaries. We leave for future work the assessment of the quantitative impact that this effect has on the accretion rate for any given choice of our model parameters.

Fourth, it has been argued that a quantum effect known as memory burden [66, 67] can suppress the evaporation rate of individual black holes once some fraction of their initial mass has evaporated [68]. The manner in which this effect would impact the cosmological dynamics of our model depends on a number of considerations which are subject to significant theoretical uncertainties, including the details of how the transition between the semi-classical and memory-burdened phases occurs [69]. We therefore leave the analysis of this effect for future work.

Fifth, in our analysis, we have focused in our analysis on effects associated with the homogeneous background cosmology. While such a treatment is generally sufficient for determining whether stasis emerges within a particular scenario and how long it lasts, given that the stasis phenomenon emerges at the level of the background cosmology, we note that in some circumstances additional effects related to spatial inhomogeneities in the energy density of a cosmological population of PBHs can modify the manner in which $f_{\rm BH}(M,t)$ evolves over time. One such effect stems from the fact that during a protracted era of PBH-domination, a perturbation δ_{Xk} in the energy density of a cosmological matter component X — including the population of PBHs itself — grows linearly with the scale factor once it enters the horizon, whereas it grows only logarithmically with a during a radiation-dominated epoch. This enhanced growth can lead to the efficient formation of self-gravitating clusters of PBHs. Within such structures, PBH binary-capture and merger rates can be significantly enhanced [70]. During an epoch of matter-radiation stasis, it has likewise been shown [23] that the growth of perturbations in a cosmological matter component which is not actively decaying or evaporating is enhanced. However, such perturbations do not grow linearly with a once they enter the horizon, but rather scale with a according to a power law of the form $\delta_{Xk} \sim a^{q(\overline{w})}$, where the power-law exponent $q(\overline{w})$ is determined [23] by the value of $\overline{w}$ and always lies within the range $0 < q(\overline{w}) < 1$. As a result, clusters of PBHs presumably can also form during an extended epoch of PBH-induced stasis, although not to the same degree as during a PBH-dominated epoch. Since merger rates are enhanced within these clusters, their formation could significantly enhance the impact that mergers have on $f_{\rm BH}(M,t)$ during stasis and eventually lead to a destabilization of the stasis dynamics. It would be interesting to consider these effects and their impact on the duration of stasis in PBH-induced stasis scenarios of this sort.

ACKNOWLEDGEMENTS

The research activities of KRD are supported in part by the U.S. Department of Energy under Grant DE-FG02-13ER41976 / DE-SC0009913 and by the U.S. National Science Foundation through its employee IR/D program. The work of LH is funded by the UK Science and Technology Facilities Council (STFC) under Grant ST/X000753/1. The research activities of FH are supported in part by ISF Grant 1784/20, by MINERVA Grant 714123, and by MINERVA Grant, Project 7141230301. The research activities of TMPT are supported in part by the U.S. National Science Foundation under Grant PHY-2210283. The research activities of BT are supported in part by the U.S. National Science Foundation under Grants PHY-2014104 and PHY-2310622. KRD and BT also wish to acknowledge the hospitality of the Center for Theoretical Underground Physics and Related Areas (CETUP*) and the Institute for Underground Science at the Sanford Underground Research Facility (SURF). The opinions and conclusions expressed herein are those of the authors and do not represent any funding agencies.

Appendix A: Probability Densities for Binary Configurations

In this Appendix, we derive the expression for $\mathcal{P}_{\rm n,nN}(M_1, M_2, M_3, x, y)$ which appears in Eq. (4.6). For pedagogical clarity, we begin by considering the idealized case wherein the spatial fluctuations in the primordial energy density are described by a Gaussian random field and the spatial distribution of PBHs whose masses lie within the range from M to $M + \Delta M$ is therefore Poissonian at all scales. We then examine how the results obtained for this idealized case are modified in the more realistic case in which the two-point correlation function $\xi(M, M', x)$ is non-vanishing.

For a population of PBHs whose spatial distribution is

Poissonian at all scales, ΔM, the comoving number density of PBHs with masses within the range M to $M+\Delta M$ is approximately $\Delta n_{\rm PBH} \approx a^3 f_{\rm BH}(M)\Delta M$. Thus, the probability that a comoving volume V contains precisely ν PBHs with masses within this range is

$$P_\nu(M,\Delta M,V) \;=\; \frac{\big[Va^3 f_{\rm BH}(M)\Delta M\big]^\nu e^{-Va^3 f_{\rm BH}(M)\Delta M}}{\nu!}~. \tag{A1}$$

Since we shall be particularly interested in comoving volumes which are either spheres or spherical shells in what follows, we introduce the compact notation

$$V(y,x) \;\equiv\; \frac{4\pi}{3}\big(y^3-x^3\big) \tag{A2}$$

for the volume of a spherical shell of outer radius y and inner radius x.

Our first step in deriving an expression for $\mathcal{P}_{\rm n,nN}(M_1,M_2,M_3,x,y)$ in this case is to determine the probability that the nearest neighbor of any given PBH of mass M_1 is located a comoving distance x away from this first PBH and has mass M_2, given the probability distribution in Eq. (A1). We begin by dividing the range of possible M_2 values into bins of width ΔM_2. We shall label these bins by a discrete index $j=0,1,2,\ldots$ such that M_{2j} denotes the minimum PBH mass in that bin. The probability that precisely one PBH with a mass within the jth bin will be located within a thin spherical shell with an inner radius x and an outer radius $x+\Delta x$ centered on the location of the first PBH is

$$\begin{aligned} P_1\big(M_{2j},\Delta M_2,V(x+\Delta x,x)\big) \;=&\\ \frac{4\pi}{3}a^3 f_{\rm BH}(M_{2j})\big[(x+\Delta x)^3-x^3\big]\Delta M_2&\\ \times\,\exp\left\{-\frac{4\pi}{3}\big[(x+\Delta x)^3-x^3\big]a^3 f_{\rm BH}(M_{2j})\Delta M_2\right\}&~. \end{aligned} \tag{A3}$$

By the same token, the probability that no additional PBHs with masses within this same bin will be located anywhere within a spherical volume of comoving radius x is

$$P_0\big(M_{2j},\Delta M_2,V(x,0)\big) \;=\; e^{-4\pi x^3 a^3 f_{\rm BH}(M_{2j})\Delta M_2/3}~. \tag{A4}$$

The joint probability of these two outcomes, which we denote $P_{1,0}(j,x,\Delta x)$, is simply the product of these individual probabilities:

$$\begin{aligned} P_{1,0}(j,x,\Delta x) \;=\; &\frac{4\pi}{3}a^3 f_{\rm BH}(M_{2j})\big[(x+\Delta x)^3-x^3\big]\Delta M_2\\ &\times e^{-4\pi(x+\Delta x)^3 a^3 f_{\rm BH}(M_{2j})\Delta M_2/3}~. \end{aligned} \tag{A5}$$

For small Δx, this expression reduces to

$$\begin{aligned} P_{1,0}(j,x,\Delta x) \;\approx\; &4\pi e^{-4\pi x^3 a^3 f_{\rm BH}(M_2)\Delta M_2/3}\\ &\times x^2 a^3 f_{\rm BH}(M_2)\Delta M_2\Delta x~. \end{aligned} \tag{A6}$$

The probability $P_{\rm N}(j,x,\Delta x)$ that the nearest neighbor of a given PBH will have a mass within the jth bin and will be located a comoving distance between x and Δx away from that other PBH is the infinite product of $P_{1,0}(j,x,\Delta x)$ for that particular value of j and the $P_0\big(M_{2j'},\Delta M_2,V(x,0)\big)$ for all other $j'\neq j$. This infinite product takes the form

$$\begin{aligned} P_{\rm N}(j,x,\Delta x) \;\approx\; &4\pi\left[\prod_{j'=0}^{\infty} e^{-4\pi x^3 a^3 f_{\rm BH}(M_{2j'})\Delta M_2/3}\right]\\ &\times x^2 a^3 f_{\rm BH}(M_{2j})\Delta M_2\Delta x~. \end{aligned} \tag{A7}$$

Expressing the product of exponentials as a sum of their arguments and taking the limit in which both $\Delta x\to 0$ and $\Delta M_2\to 0$, we obtain the differential probability that a given PBH has a nearest neighbor within the infinitesimal mass range from M_2 to M_2+dM_2 and comoving-distance range x to $x+dx$. Expressing this differential probability in terms of the corresponding probability density $\mathcal{P}_{\rm N}(M_2,x)$, we have

$$\begin{aligned} \mathcal{P}_{\rm N}(M_2,x)dM_2dx \;=&\\ 4\pi\exp\left[-\frac{4\pi}{3}x^3a^3\int_0^\infty f_{\rm BH}(M)dM\right]&\\ \times x^2a^3 f_{\rm BH}(M_2)dM_2dx~.& \end{aligned} \tag{A8}$$

Given a particular combination of M_2 and x for the nearest neighbor, we also wish to determine the probability that the next-to-nearest neighbor of a given PBH has mass M_3 and is located a comoving distance $y>x$ away from this first PBH. Proceeding as above, we begin by dividing the range of possible M_3 values into bins of width ΔM_3 and labeling these bins by a discrete index j. The probability that precisely one PBH with a mass within the jth bin will be located within a thin spherical shell with inner radius y and outer radius $y+\Delta y$ centered on the first PBH is

$$\begin{aligned} P_1\big(M_{3j},\Delta M_3,V(y+\Delta y,y)\big) \;=&\\ \frac{4\pi}{3}a^3 f_{\rm BH}(M_{3j})\Delta M_3\big[(y+\Delta y)^3-y^3\big]&\\ \times\,\exp\left\{-\frac{4\pi}{3}\big[(y+\Delta y)^3-y^3\big]a^3 f_{\rm BH}(M_{3j})\Delta M_3\right\}&~. \end{aligned} \tag{A9}$$

The probability that no additional PBHs with masses in this same bin are located within a (not necessarily thin) spherical shell with inner radius x and outer radius y is

$$P_0\big(M_{3j},\Delta M_3,V(y,x)\big) \;=\; e^{-4\pi(y^3-x^3)a^3 f_{\rm BH}(M_{3j})\Delta M_3/3}~. \tag{A10}$$

For small Δy, the joint probability $P_{1,0}(j,y,x,\Delta y)$ of these two outcomes is approximately

$$\begin{aligned} P_{1,0}\big(j,y,x,\Delta y\big) \;\approx\; &4\pi e^{-4\pi(y^3-x^3)a^3 f_{\rm BH}(M_{3j})\Delta M_3/3}\\ &\times y^2a^3 f_{\rm BH}(M_{3j})\Delta M_3\Delta y~. \end{aligned} \tag{A11}$$

The probability $P_{\rm nN}(j, y, x, \Delta y)$ that the next-to-nearest neighbor of a given PBH with a nearest neighbor located a comoving distance x away from it will have a mass within the jth bin and will be located a comoving distance between y and $y + \Delta y$ away from it is the infinite product of $P_{1,0}(j, y, x, \Delta y)$ for that particular value of j and the $P_0\big(j', V(x, y)\big)$ for all other $j' \neq j$. This infinite product takes the form

$$P_{\rm nN}(j, y, \Delta y) \;\approx\; 4\pi \left[\prod_{j'=0}^{\infty} e^{-4\pi(y^3-x^3)a^3 f_{\rm BH}(M_{3j'})\Delta M_3/3}\right] \times y^2 a^3 f_{\rm BH}(M_{3j})\Delta M_3 \Delta y \;. \quad \text{(A12)}$$

Expressing the product of exponentials as a sum of their arguments and taking the limit in which both $\Delta y \to 0$ and $\Delta M_3 \to 0$, we obtain the differential probability that a given PBH has a next-to-nearest neighbor within the infinitesimal mass range from M_3 to $M_3 + dM_3$ and comoving-distance range y to $y+dy$. Expressing this differential probability in terms of the corresponding probability density $\mathcal{P}_{\rm N}(M_3, y)$, we have

$$\mathcal{P}_{\rm N}(M_3, y) dM_3 dy \;=\; 4\pi \exp\left[-\frac{4\pi}{3}(y^3 - x^3)a^3 \int_0^\infty f_{\rm BH}(M)dM\right] \times y^2 a^3 f_{\rm BH}(M_3) dM_3 dy \;. \quad \text{(A13)}$$

The joint probability density $\mathcal{P}_{n,nN}(M_1, M_2, M_3, x, y)$ that the nearest neighbor of a particular PBH of mass M_1 will be located a comoving distance x away from that first PBH, that the next-to-nearest neighbor of that same PBH will be located a distance y away from that first PBH, and that these two PBHs will have masses M_2 and M_3, respectively, is the product of the probability densities in Eqs. (A8) and Eq. (A13):

$$\mathcal{P}_{\rm n,nN}(M_1, M_2, M_3, x, y) \;=\; 16\pi^2 x^2 y^2 \exp\left[-\frac{4\pi}{3} y^3 a^3 \int_0^\infty f_{\rm BH}(M)dM\right] \times a^6 f_{\rm BH}(M_2) f_{\rm BH}(M_3) \;. \quad \text{(A14)}$$

For a population of PBHs which are perfectly Poisson-distributed, the two-point correlation function is simply $\xi(M, M', x) = 0$, as discussed above. Thus, for such a population of PBHs, the expression in Eq. (4.5) reduces to

$$N(M', y) \;=\; \frac{4\pi}{3} y^3 a^3 \int_0^\infty f_{\rm BH}(M)dM \;, \quad \text{(A15)}$$

which is independent of the value of M'. Thus, for such a population of PBHs, we may express $\mathcal{P}_{\rm n,nN}(M_1, M_2, M_3, x, y)$ in terms of the quantities defined in Eqs. (4.3) and (4.5) as

$$\mathcal{P}_{\rm n,nN}(M_1, M_2, M_3, x, y) \;=\; e^{-N(M_1,y)} \frac{\partial^2 N(M_2, M_1, x)}{\partial M_2 \partial x} \frac{\partial^2 N(M_3, M_1, y)}{\partial M_3 \partial y} \;, \quad \text{(A16)}$$

which is independent of M_1.

While the expression in Eq. (A16) is strictly valid only for a perfectly spatially homogeneous, Poisson-distributed population of PBHs, this result can be generalized in a straightforward manner to the case in which the correlation function $\xi(M, M', x)$ is non-vanishing [45]. The corresponding expression for the joint probability density in this case may be obtained by replacing the expression for $V(y, x)$ in Eq. (A2) with

$$V(M, M', y, x) \;\equiv\; 4\pi \int_x^y \big[1+\xi(M, M', z)\big] z^2 dz \;. \quad \text{(A17)}$$

One can then derive an expression for $\mathcal{P}_{\rm n,nN}(M_1, M_2, M_3, x, y)$ in a manner analogous to the manner in which we have derived the corresponding result for the purely Poisson case. Noting that the fundamental theorem of calculus implies that

$$\lim_{\Delta x \to 0} V(M, M', x + \Delta x, x) \;=\; 4\pi\big[1 + \xi(M, M', x)\big] x^2 dx \quad \text{(A18)}$$

for a spherical shell of infinitesimal width, we find that $\mathcal{P}_{\rm n,nN}(M_1, M_2, M_3, x, y)$ is given by an expression of exactly the same form as the expression Eq. (A16), but in which $\partial N(M_2, M_1, x)/dM_2 dx$ and $\partial N(M_3, M_1, x)/dM_2 dx$ include the full expressions for $\xi(M_2, M_1, x)$ and $\xi(M_3, M_1, y)$, respectively, and in which the expression in Eq. (A15) is modified to

$$N(M', y) \;=\; 4\pi a^3 \int_0^y dx\, x^2 \int_0^\infty dM \Big\{ f_{\rm BH}(M) \times \big[1 + \xi(M, M', x)\big]\Big\} \;, \quad \text{(A19)}$$

which has the form as the expression in Eq. (4.5) for non-vanishing $\xi(M, M', x)$.

[1] A. M. Green, Fundam. Theor. Phys. **178**, 129 (2015), arXiv:1403.1198 [gr-qc].
[2] A. Escrivà, F. Kuhnel, and Y. Tada, (2022), arXiv:2211.05767 [astro-ph.CO].
[3] S. Hawking, Mon. Not. Roy. Astron. Soc. **152**, 75 (1971).
[4] G. F. Chapline, Nature **253**, 251 (1975).
[5] D. Baumann, P. J. Steinhardt, and N. Turok, (2007), arXiv:hep-th/0703250.
[6] T. Fujita, M. Kawasaki, K. Harigaya, and R. Matsuda, Phys. Rev. D **89**, 103501 (2014), arXiv:1401.1909 [astro-ph.CO].
[7] O. Lennon, J. March-Russell, R. Petrossian-Byrne, and

H. Tillim, JCAP **04**, 009 (2018), arXiv:1712.07664 [hep-ph].
[8] R. Allahverdi, J. Dent, and J. Osinski, Phys. Rev. D **97**, 055013 (2018), arXiv:1711.10511 [astro-ph.CO].
[9] L. Morrison, S. Profumo, and Y. Yu, JCAP **05**, 005 (2019), arXiv:1812.10606 [astro-ph.CO].
[10] D. Hooper, G. Krnjaic, and S. D. McDermott, JHEP **08**, 001 (2019), arXiv:1905.01301 [hep-ph].
[11] I. Masina, Eur. Phys. J. Plus **135**, 552 (2020), arXiv:2004.04740 [hep-ph].
[12] I. Baldes, Q. Decant, D. C. Hooper, and L. Lopez-Honorez, JCAP **08**, 045 (2020), arXiv:2004.14773 [astro-ph.CO].
[13] B. Batell *et al.*, Int. J. Mod. Phys. A **40**, 2530004 (2025), arXiv:2411.04780 [astro-ph.CO].
[14] J. D. Barrow, E. J. Copeland, and A. R. Liddle, Mon. Not. Roy. Astron. Soc. **253**, 675 (1991).
[15] K. R. Dienes, L. Heurtier, F. Huang, D. Kim, T. M. P. Tait, and B. Thomas, (2022), arXiv:2212.01369 [astro-ph.CO].
[16] K. R. Dienes, L. Heurtier, F. Huang, D. Kim, T. M. P. Tait, and B. Thomas, Phys. Rev. D **105**, 023530 (2022), arXiv:2111.04753 [astro-ph.CO].
[17] K. R. Dienes, L. Heurtier, F. Huang, T. M. P. Tait, and B. Thomas, Phys. Rev. D **109**, 083508 (2024), arXiv:2309.10345 [astro-ph.CO].
[18] K. R. Dienes, L. Heurtier, F. Huang, T. M. P. Tait, and B. Thomas, Phys. Rev. D **110**, 123514 (2024), arXiv:2406.06830 [astro-ph.CO].
[19] J. Halverson and S. Pandya, Phys. Rev. D **110**, 075041 (2024), arXiv:2408.00835 [astro-ph.CO].
[20] J. Barber, K. R. Dienes, and B. Thomas, Phys. Rev. D **110**, 123515 (2024), arXiv:2408.16255 [astro-ph.CO].
[21] J. Barber, K. R. Dienes, and B. Thomas, Phys. Rev. D **111**, 063519 (2025), arXiv:2412.09123 [astro-ph.CO].
[22] F. Huang and V. Knapp-Perez, JHEP **09**, 072 (2025), arXiv:2502.20449 [hep-ph].
[23] K. R. Dienes, L. Heurtier, D. Hoover, F. Huang, A. Paulsen, and B. Thomas, (2025), arXiv:2503.19959 [astro-ph.CO].
[24] A. J. Long, B. Shams Es Haghi, and M. Venegas, (2025), arXiv:2506.04502 [hep-ph].
[25] C. T. Byrnes and P. S. Cole (2021) arXiv:2112.05716 [astro-ph.CO].
[26] J. H. MacGibbon and B. R. Webber, Phys. Rev. **D41**, 3052 (1990).
[27] J. H. MacGibbon, Phys. Rev. **D44**, 376 (1991).
[28] B. J. Carr, Astrophys. J. **201**, 1 (1975).
[29] A. M. Green and A. R. Liddle, Phys. Rev. D **56**, 6166 (1997), arXiv:astro-ph/9704251.
[30] H. I. Kim, C. H. Lee, and J. H. MacGibbon, Phys. Rev. D **59**, 063004 (1999), arXiv:astro-ph/9901030.
[31] T. Bringmann, C. Kiefer, and D. Polarski, Phys. Rev. D **65**, 024008 (2002), arXiv:astro-ph/0109404.
[32] B. Carr, M. Raidal, T. Tenkanen, V. Vaskonen, and H. Veermäe, Phys. Rev. D **96**, 023514 (2017), arXiv:1705.05567 [astro-ph.CO].
[33] B. J. Carr, K. Kohri, Y. Sendouda, and J. Yokoyama, Phys. Rev. D **81**, 104019 (2010), arXiv:0912.5297 [astro-ph.CO].
[34] B. Carr, K. Kohri, Y. Sendouda, and J. Yokoyama, (2020), arXiv:2002.12778 [astro-ph.CO].
[35] C. Keith, D. Hooper, N. Blinov, and S. D. McDermott, Phys. Rev. D **102**, 103512 (2020), arXiv:2006.03608 [astro-ph.CO].
[36] Y. Akrami *et al.* (Planck), Astron. Astrophys. **641**, A10 (2020), arXiv:1807.06211 [astro-ph.CO].
[37] M. Raidal, V. Vaskonen, and H. Veermäe, JCAP **09**, 037 (2017), arXiv:1707.01480 [astro-ph.CO].
[38] N. Aghanim *et al.* (Planck), Astron. Astrophys. **641**, A6 (2020), [Erratum: Astron.Astrophys. 652, C4 (2021)], arXiv:1807.06209 [astro-ph.CO].
[39] T. Nakamura, M. Sasaki, T. Tanaka, and K. S. Thorne, Astrophys. J. Lett. **487**, L139 (1997), arXiv:astro-ph/9708060.
[40] K. Ioka, T. Chiba, T. Tanaka, and T. Nakamura, Phys. Rev. D **58**, 063003 (1998), arXiv:astro-ph/9807018.
[41] Y. Ali-Haïmoud, E. D. Kovetz, and M. Kamionkowski, Phys. Rev. D **96**, 123523 (2017), arXiv:1709.06576 [astro-ph.CO].
[42] P. C. Peters, Phys. Rev. **136**, B1224 (1964).
[43] M. Sasaki, T. Suyama, T. Tanaka, and S. Yokoyama, Phys. Rev. Lett. **117**, 061101 (2016), [Erratum: Phys.Rev.Lett. 121, 059901 (2018)], arXiv:1603.08338 [astro-ph.CO].
[44] V. Desjacques and A. Riotto, Phys. Rev. D **98**, 123533 (2018), arXiv:1806.10414 [astro-ph.CO].
[45] G. Ballesteros, P. D. Serpico, and M. Taoso, JCAP **10**, 043 (2018), arXiv:1807.02084 [astro-ph.CO].
[46] P. Auclair and B. Blachier, (2024), arXiv:2402.00600 [astro-ph.CO].
[47] M. Ricotti, Astrophys. J. **662**, 53 (2007), arXiv:0706.0864 [astro-ph].
[48] M. Ricotti, J. P. Ostriker, and K. J. Mack, Astrophys. J. **680**, 829 (2008), arXiv:0709.0524 [astro-ph].
[49] J. R. Rice and B. Zhang, JHEAp **13-14**, 22 (2017), arXiv:1702.08069 [astro-ph.HE].
[50] V. De Luca, G. Franciolini, P. Pani, and A. Riotto, JCAP **04**, 052 (2020), arXiv:2003.02778 [astro-ph.CO].
[51] V. De Luca, G. Franciolini, P. Pani, and A. Riotto, Phys. Rev. D **102**, 043505 (2020), arXiv:2003.12589 [astro-ph.CO].
[52] V. De Luca, G. Franciolini, P. Pani, and A. Riotto, JCAP **06**, 044 (2020), arXiv:2005.05641 [astro-ph.CO].
[53] H. Bondi, Mon. Not. Roy. Astron. Soc. **112**, 195 (1952).
[54] Y. B. Zel'dovich and I. D. Novikov, Sov. Astron. **10**, 602 (1967).
[55] E. Babichev, V. Dokuchaev, and Y. Eroshenko, Phys. Rev. Lett. **93**, 021102 (2004), arXiv:gr-qc/0402089.
[56] E. Babichev, V. Dokuchaev, and Y. Eroshenko, J. Exp. Theor. Phys. **100**, 528 (2005), arXiv:astro-ph/0505618.
[57] E. Bertschinger, Astrophys. J. Suppl. **58**, 39 (1985).
[58] E. de Jong, J. C. Aurrekoetxea, and E. A. Lim, JCAP **03**, 029 (2022), arXiv:2109.04896 [astro-ph.CO].
[59] V. De Luca, G. Franciolini, A. Kehagias, P. Pani, and A. Riotto, Phys. Lett. B **832**, 137265 (2022), arXiv:2112.02534 [astro-ph.CO].
[60] B. J. Carr and S. W. Hawking, Mon. Not. Roy. Astron. Soc. **168**, 399 (1974).
[61] B. J. Carr, T. Harada, and H. Maeda, Class. Quant. Grav. **27**, 183101 (2010), arXiv:1003.3324 [gr-qc].
[62] G. V. Bicknell and R. N. Henriksen, Astrophys. J. **225**, 237 (1978).
[63] P. S. Custodio and J. E. Horvath, Phys. Rev. D **58**, 023504 (1998), arXiv:astro-ph/9802362.
[64] T. Harada and B. J. Carr, Phys. Rev. D **71**, 104010 (2005), arXiv:astro-ph/0412135.
[65] T. Harada and B. J. Carr, Phys. Rev. D **71**, 104009

(2005), arXiv:astro-ph/0412134.
[66] G. Dvali, (2018), arXiv:1810.02336 [hep-th].
[67] G. Dvali, L. Eisemann, M. Michel, and S. Zell, JCAP **03**, 010 (2019), arXiv:1812.08749 [hep-th].
[68] G. Dvali, L. Eisemann, M. Michel, and S. Zell, Phys. Rev. D **102**, 103523 (2020), arXiv:2006.00011 [hep-th].
[69] G. Montefalcone, D. Hooper, K. Freese, C. Kelso, F. Kuhnel, and P. Sandick, (2025), arXiv:2503.21005 [astro-ph.CO].
[70] I. Holst, G. Krnjaic, and H. Xiao, (2024), arXiv:2412.01890 [astro-ph.CO].